J|A|C|S ARTICLES

Published on Web 02/24/2009

Unprecedented Binding Cooperativity between Cu^{I} and Cu^{II} in the Copper Resistance Protein CopK from *Cupriavidus metallidurans* CH34: Implications from Structural Studies by NMR Spectroscopy and X-Ray Crystallography

Lee Xin Chong,[†] Miriam-Rose Ash,[‡] Megan J. Maher,[*,§] Mark G. Hinds,[*,||] Zhiguang Xiao,[*,†] and Anthony G. Wedd[†]

School of Chemistry and, Biomolecular Science and Biotechnology Institute, University of Melbourne, Parkville, Victoria 3010, Australia, The Walter and Eliza Hall Institute of Medical Research, Parkville, Victoria 3052 Australia, Centenary Institute of Cancer Medicine and Cell Biology, Locked Bag No. 6, Newtown, NSW, 2042, Australia, and School of Molecular and Microbial Sciences, University of Sydney, NSW, 2006, Australia

Received September 17, 2008; E-mail: z.xiao@unimelb.edu.au; m.maher@centenary.org.au; mhinds@wehi.edu.au

Abstract: The bacterium *Cupriavidus metallidurans* CH34 is resistant to high environmental concentrations of many metal ions, including copper. This ability arises primarily from the presence of a large plasmid pMOL30 which includes a cluster of 19 *cop* genes that respond to copper. One of the protein products CopK is induced at high levels and is expressed to the periplasm as a small soluble protein (8.3 kDa). *Apo*-CopK associates in solution to form a dimer ($K_D \approx 10^{-5}$ M) whose structure was defined by NMR and X-ray crystallography. The individual molecules feature two antiparallel β-sheets arranged in a sandwich-like structure and interact through C-terminal β-strands. It binds Cu^{II} with low affinity ($K_D(Cu^{II}) > 10^{-6}$ M) but Cu^{I} with high affinity ($K_D(Cu^{I}) = 2 \times 10^{-11}$ M). Cu^{I}−CopK was also a dimer in the solid state and featured a distorted tetrahedral site $Cu^{I}(S\text{-}Met)_3(NCS)$. The isothiocyanato ligand originated from the crystallization solution. Binding of Cu^{I} or Ag^{I}, but not of Cu^{II}, favored the monomeric form in solution. While Ag^{I}−CopK was stable as isolated, Cu^{I}−CopK was moderately air-sensitive due to a strong binding cooperativity between Cu^{I} and Cu^{II}. This was documented by determination of the Cu^{I} and Cu^{II} binding affinities in the presence of the other ion: $K_D(Cu^{I}) = 2 \times 10^{-13}$ M and $K_D(Cu^{II}) = 3 \times 10^{-12}$ M, that is, binding of Cu^{II} increased the affinity for Cu^{I} by a factor of $\sim 10^2$ and binding of Cu^{I} increased the affinity for Cu^{II} by a factor of at least 10^6. Stable forms of both $Cu^{I}Cu^{II}$−CopK and $Ag^{I}Cu^{II}$−CopK were isolated readily. Consistent with this unprecedented copper binding chemistry, NMR spectroscopy detected three distinct forms: *apo*-CopK, Cu^{I}−CopK and $Cu^{I}Cu^{II}$−CopK that do not exchange on the NMR time scale. This information provides a valuable guide to the role of CopK in copper resistance.

Introduction

Fluctuations in nutrient copper levels in the micromolar range are controlled in gram negative bacteria by chromosomal tolerance operons which include two key regulation systems.[1] The first involves two proteins: CopA, a P-type ATPase which transports excess Cu^{I} from the cytoplasm to the periplasm where it is oxidized by CueO, a multicopper oxidase.[2−5] The second system, CusCFBA, comprises a tripartite protein complex CusCBA that spans the complete cell wall as a proton-substrate antiporter and a fourth member CusF.[6] This system confers copper tolerance by expelling Cu^{I} directly from the periplasm, a role performed primarily under anaerobic conditions.[6,7]

High environmental copper levels have led to copper-resistant bacteria that can survive at millimolar concentrations of copper. These strains possess additional plasmid-borne operons that confer this resistance.[1] Among the better documented examples are *pco* and *cop* operons that were found, respectively, in strains of *Escherichia coli* isolated from the faeces of copper-fed pigs and of *Pseudomonas syringae* pathovar *tomato* isolated from plants exposed to high levels of antifungal copper compounds.[8,9] The *pco* operon comprises seven genes, *pcoABCDpcoRSpcoE*, and expresses resistance proteins PcoABCDE that are regulated by the two-component system PcoRS.[10−12] Three soluble

[†] University of Melbourne.
[‡] University of Sydney.
[§] Centenary Institute of Cancer Medicine and Cell Biology.
[||] The Walter and Eliza Hall Institute of Medical Research.

(1) Rensing, C.; Grass, G. *FEMS Microbiol. Rev.* **2003**, *27*, 197–213.
(2) Rensing, C.; Fan, B.; Sharma, R.; Mitra, B.; Rosen, B. P. *Proc. Natl. Acad. Sci. U.S.A.* **2000**, *97*, 652–656.
(3) Kim, C.; Lorenz, W. W.; Hoopes, J. T.; Dean, J. F. *J. Bacteriol.* **2001**, *183*, 4866–4875.
(4) Singh, S. K.; Grass, G.; Rensing, C.; Montfort, W. R. *J. Bacteriol.* **2004**, *186*, 7815–7817.
(5) Grass, G.; Rensing, C. *Biochem. Biophys. Res. Commun.* **2001**, *286*, 902–908.
(6) Franke, S.; Grass, G.; Rensing, C.; Nies, D. H. *J. Bacteriol.* **2003**, *185*, 3804–3812.
(7) Outten, F. W.; Huffman, D. L.; Hale, J. A.; O'Halloran, T. V. *J. Biol. Chem.* **2001**, *276*, 30670–30677.
(8) Tetaz, T. J.; Luke, R. K. *J. Bacteriol.* **1983**, *154*, 1263–1268.
(9) Cooksey, D. A. *FEMS Microbiol. Rev.* **1994**, *14*, 381–386.
(10) Rouch, D. A.; Brown, N. L. *Microbiology* **1997**, *143*, 1191–1202.

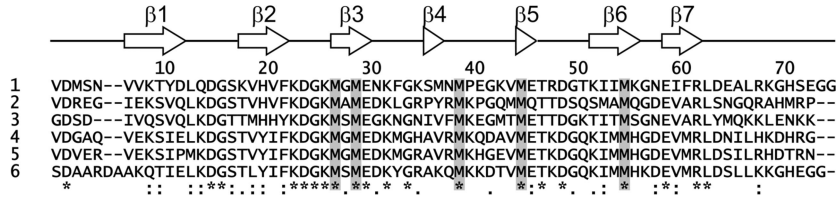

Figure 1. Multiple-sequence alignment of partial sequences of proteins homologous to CopK. Residue numbering refers to the sequence of CopK excluding the leader sequence. Shown in the alignment are the sequences of following proteins: (1) CopK from *Cupriavidus metallidurans* CH34 (YP_145685, residues 21−94); (2) *Polaromonas naphthalenivorans* CJ2 (YP_973570, residues 22−93); (3) *Rhodoferax ferrireducens* T118 (YP_521702, residues 23−93); (4) *Dechloromonas aromatica* RCB (YP_285489: residues 21−92; (5) *Thauera* sp. MZ1T (ZP_02843547, residues 21−92); (6) *Acidovorax sp.* JS42 (YP_986936: residues 21−95). The conserved methionines are identified by gray shading and the secondary structure elements as determined from the crystal structure of *apo*-CopK are shown above the CopK sequence.

proteins (PcoA, PcoC, PcoE) are expressed to the periplasm and two copper pumps (PcoB, PocD) are present in the outer and inner membranes, respectively.[11] PcoA is a multicopper oxidase with cuprous oxidase activity.[13,14] PcoC is a copper chaperone with two separate binding sites specific for Cu^{I} and Cu^{II}.[15] The protein loaded with both copper ions (i.e., $Cu^{I}Cu^{II}$−PcoC) is air-stable, but PcoA catalyzes air-oxidation of the Cu^{I} bound in $Cu^{I}Cu^{II}$−PcoC to less toxic Cu^{2+}.[13] The *cop* operons found in *P. syringae* and other copper resistance bacteria feature equivalent gene structures and highly homologous protein products, suggesting a conserved mechanism of copper resistance.[15−18]

The bacterium *Cupriavidus metallidurans* CH34 was isolated from sediments of a zinc decantation basin in Belgium and is highly tolerant to the presence of many heavy metal ions including copper.[19] Its copper resistance was attributed to a more complex *cop* cluster consisting of 19 genes (*copVTMKNSRABCDIJGFLQHE*) present on a large plasmid pMOL30.[19,20] Expression of all 19 genes was up-regulated by copper salts and the expression level of each depended on both copper concentration and exposure time.[20] The products of the *cop* cluster include proteins homologous to those of the *pco/cop* operons discussed above. In addition, there is a transmembrane P1-type ATPase CopF and several cysteine-containing cytosolic proteins (CopJ, CopG, CopL) that may work collectively to remove Cu^{I} from the cytosol. This, in turn, may require extra copper-binding proteins to handle the increased copper stress in the periplasm. In fact, there are several periplasmic proteins that are unique to this system. One of them is CopK which accumulated to very high levels in the periplasm when the cells were challenged with high copper concentrations.[20]

Recently, the solution structure of *apo*-CopK was described and it was reported that the monomeric form can bind two Cu^{+} ions with different affinities.[21] A BLAST search for homologous proteins identified five other hypothetical proteins with >40% sequence identity to CopK (Figure 1). However, among this group of proteins, CopK is the only one that has been isolated and its biological function investigated. We show here that the CopK species that contains two Cu ions is, in fact, $Cu^{I}Cu^{II}$−CopK, formed as a consequence of cooperativity in binding Cu^{I} and Cu^{II} at separated sites under oxidizing conditions. Cu^{I} binding enhances the specific affinity for Cu^{II} by a factor of at least 10^{6} while, in turn, Cu^{II} binding increases the specific affinity for Cu^{I} by a factor of about 10^{2}. This behavior is unprecedented in copper binding proteins. The structural implications of metal binding were explored by both NMR spectroscopy and X-ray crystallography and the combined data allow a discussion of the potential role of CopK in copper resistance.

Results and Discussion

Protein Expression and Characterization. A synthetic gene for CopK from *C. metallidurans* CH34 (including the leader sequence) was assembled by PCR with codons optimized for expression in *E. coli*. The leader sequence was processed correctly by the expression host to produce the mature form of wild type CopK protein that was purified readily by conventional chromatography (Figure S1, Supporting Information). The experimental molar mass of the *apo* protein determined by electrospray ionization mass spectrometry (ESI-MS) was 8280 Da (Figure S2, Supporting Information). A value of 8279.5 Da is predicted for a CopK protein with the N-terminal sequence VDMSN defined previously for protein isolated from its native host.[20]

CopK is expressed in *C. metallidurans* CH34 in response to elevated levels of copper and is likely to be involved in copper sequestration and/or transportation. The interaction between Cu^{2+} and CopK can be monitored conveniently by spectroscopy. *Apo*-CopK fluoresces (λ_{ex}, 280 nm; λ_{em}, 309 nm) due to the presence of a single tyrosine residue Tyr10. Addition of paramagnetic Cu^{2+} to *apo*-CopK (50 μM) in the buffer 3-(*N*-morpholino)propanesulfonic acid (Mops) (20 mM; pH 7) which has a weak affinity for Cu^{II} ($K_D(Cu^{II}) = 10^{-4}$ M)[22] caused quenching of the fluorescence intensity but no clear end point

(11) Brown, N. L.; Barrett, S. R.; Camakaris, J.; Lee, B. T.; Rouch, D. A. *Mol. Microbiol.* **1995**, *17*, 1153–1166.
(12) Rouch, D.; Camakaris, J.; Lee, B. T.; Luke, R. K. *J. Gen. Microbiol.* **1985**, *131*, 939–943.
(13) Djoko, K. Y.; Xiao, Z.; Wedd, A. G. *ChemBioChem* **2008**, *9*, 1579–1582.
(14) Huffman, D. L.; Huyett, J.; Outten, F. W.; Doan, P. E.; Finney, L. A.; Hoffman, B. M.; O'Halloran, T. V. *Biochemistry* **2002**, *41*, 10046–10055.
(15) Djoko, K. Y.; Xiao, Z.; Huffman, D. L.; Wedd, A. G. *Inorg. Chem.* **2007**, *46*, 4560–4568.
(16) Drew, S. C.; Djoko, K. Y.; Zhang, L.; Koay, M.; Boas, J. F.; Pilbrow, J. R.; Xiao, Z.; Barnham, K. J.; Wedd, A. G. *J. Biol. Inorg. Chem.* **2008**, *13*, 899–907.
(17) Zhang, L.; Koay, M.; Maher, M. J.; Xiao, Z.; Wedd, A. G. *J. Am. Chem. Soc.* **2006**, *128*, 5834–5850.
(18) Koay, M.; Zhang, L.; Yang, B.; Maher, M. J.; Xiao, Z.; Wedd, A. G. *Inorg. Chem.* **2005**, *44*, 5203–5205.
(19) Mergeay, M.; Monchy, S.; Vallaeys, T.; Auquier, V.; Benotmane, A.; Bertin, P.; Taghavi, S.; Dunn, J.; van der Lelie, D.; Wattiez, R. *FEMS Microbiol. Rev.* **2003**, *27*, 385–410.
(20) Monchy, S.; Benotmane, M. A.; Wattiez, R.; van Aelst, S.; Auquier, V.; Borremans, B.; Mergeay, M.; Taghavi, S.; van der Lelie, D.; Vallaeys, T. *Microbiology* **2006**, *152*, 1765–1776.
(21) Bersch, B.; Favier, A.; Schanda, P.; van Aelst, S.; Vallaeys, T.; Covès, J.; Mergeay, M.; Wattiez, R. *J. Mol. Biol.* **2008**, *380*, 386–403.
(22) Magyar, J. S.; Godwin, H. A. *Anal. Biochem.* **2003**, *320*, 39–54.

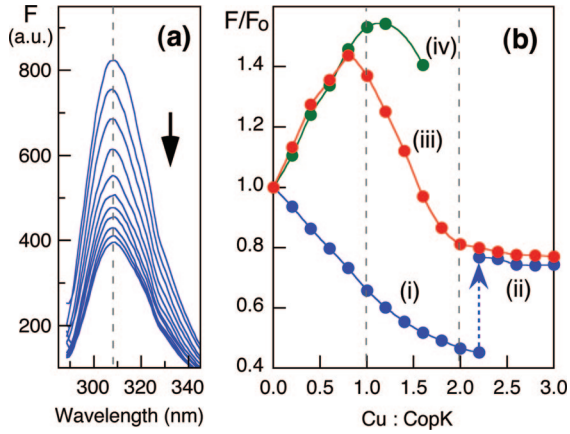

Figure 2. (a) Quenching of fluorescence emission intensity for *apo*-CopK (50 μM) in Mops buffer (20 mM; pH 7; NaCl, 100 mM) upon titration with copper solutions (2.0 mM). (b) Plots of emission intensity at 310 nm relative to that of *apo*-CopK (F/F_o) as a function of Cu:CopK ratio upon titration with: (i) Cu^{2+}; (ii) further titration of solution (i) with Cu^{2+} after addition of NH_2OH (1.0 mM) at Cu:CopK = 2.2; (iii) as for solution (i) with NH_2OH (1.0 mM) in the buffer; (iv) $[Cu^I[CH_3CN)_4]^+$ under anaerobic conditions.

(Figure 2a, b(i)). Equivalent titrations in the buffer Na-Tricine (where Tricine = *N*-(2-Hydroxy-1,1-bis(hydroxymethyl)ethyl)glycine) (20 mM, pH 7) which has a higher affinity for Cu^{II} ($K_D(Cu^{II}) = 10^{-6.1}$ M)[22] or by Cu^{II}(Edta) (where Edta = ethylenediamine-*N*,*N*,*N*′,*N*′-tetraacetic acid) in place of free Cu^{+2} led to similar quenching but at reduced levels (~70 and ~25%, respectively). The data are consistent with dynamic quenching by paramagnetic Cu^{II} complexes in solution and a weak interaction between *apo*-CopK and Cu^{2+} (estimated $K_D(Cu^{II}) > 10^{-6}$ M). The Cu^{II} ions in the weakly associated "Cu^{II}−CopK" species were removed quantitatively by a simple desalting column with recovery of *apo* protein.

When the titration equivalent to that of Figure 2b(i) was carried out in Mops buffer that contained weak reductant NH_2OH, a distinctly different pattern of change in fluorescence intensity was observed (Figure 2b(iii)). The intensity increased initially in the range Cu:CopK = 0 − 0.8, but diminished subsequently with two apparent turning-points at Cu:CopK = 0.8 and 2, respectively. Removal of unbound copper on a gel filtration column led to the isolation of a stable protein of stoichiometry Cu^I:Cu^{II}:CopK = 1:1:1 (designated as Cu^ICu^{II}−CopK; see Table 2 below). Addition of NH_2OH into the solution of titration 2b(i) at Cu:CopK = 2.2 led to an increase in the fluorescence intensity to match that of titration 2b(iii) (Figure 2b(ii)) and Cu^ICu^{II}−CopK was also isolated cleanly from this solution. Addition of NH_2OH into an equivalent solution that contained Cu^{2+} as Cu^{II}(Edta) caused no change in the fluorescence intensity and the protein was recovered as *apo*-CopK only. It is apparent that there exists a high affinity Cu^I site on CopK that promotes reductive trapping of labile Cu^{2+} as bound Cu^I. Binding of Cu^I enhanced the affinity of the protein for Cu^{II} (by a factor of at least 10^6; see below). This effect allowed ready isolation of stable Cu^ICu^{II}−CopK as the only protein product under the conditions.

Titration of *apo*-CopK (50 μM) with $[Cu^I(CH_3CN)_4]^+$ under anaerobic conditions led to an initial linear increase in the emission intensity to match that of titration 2b(iii). The increase leveled off at Cu^I:CopK = 1 (Figure 2b(iv)). However, solutions with Cu^I:CopK > 1 were air-sensitive and the emission intensity dropped readily with excess Cu^I and, again, only stable

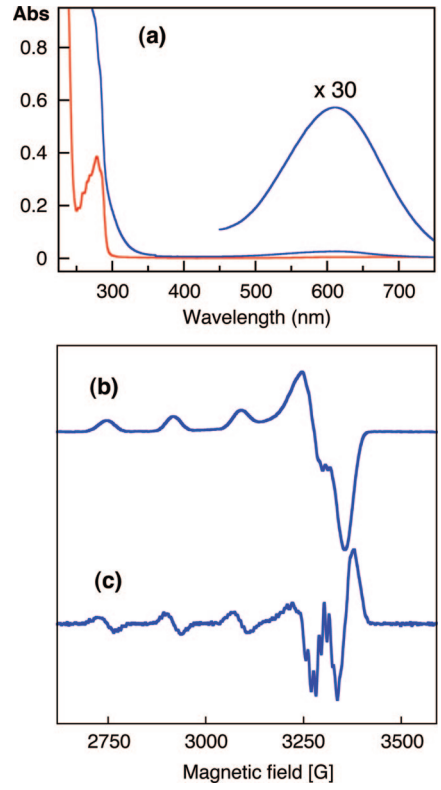

Figure 3. (a) Solution spectra of Cu^ICu^{II}−CopK (0.25 mM; blue) and *apo*-CopK (0.25 mM; red) in Mops buffer (20 mM; pH 7; NaCl, 100 mM); (b) frozen EPR spectrum of Cu^ICu^{II}−CopK (1.0 mM) in Mops buffer (50 mM, pH 7; NaCl, 100 mM; 10% (v/v) glycerol); (c) second derivative EPR spectrum emphasizing superhyperfine coupling to ^{14}N nuclei. Conditions of measurement: temperature, 77 K; frequency, 9.42 GHz; microwave power, 5.3 mW; modulation frequency, 100 kHz; modulation amplitude, 0.4 mT; time constant, 0.16 s.

Cu^ICu^{II}−CopK was isolated from solutions after gel-filtration chromatography in air. Cu^+ is a diamagnetic d^{10} metal ion but its binding to CopK enhanced the emission efficiency of Tyr 10 (Figure 2b(iii), (iv)). The behavior suggested that specific binding by diamagnetic Cu^I induced a significant structural change in solution whereas the weak interactions with paramagnetic Cu^{2+} had no such effect. A quantitative analysis is given below. Equivalent titrations monitored by UV absorbance spectroscopy provided complimentary information that was also consistent with cooperative binding of Cu^I and Cu^{II} (Figure S3, Supporting Information).

Concentrated samples of Cu^ICu^{II}−CopK were light blue due to a weak absorbance maximum at 610 nm ($\epsilon = 82$ M^{-1} cm^{-1}), assigned to the *d*-*d* transition typical of bound Cu^{II} in type 2 copper centers with coordination spheres of oxygen and/or nitrogen atoms (Figure 3a).[23] The frozen-glass EPR spectrum was also characteristic of a type 2 center with $g_{||} = 2.24$, $A_{||} = 18 \times 10^{-3}$ cm^{-1} and $g_\perp = 2.03$ (Figure 3b).[23] Superhyperfine structure attributable to coupling of $^{63}Cu/^{65}Cu$ ($I = 3/2$) to at least one ^{14}N nucleus ($I = 1$) was detected in both the parallel and perpendicular directions (Figure 3c). Either or both of the two residues His 19 and His 70 in the CopK sequence may act as Cu^{II} ligands with the further possibility of backbone amide ligands, including the N-terminus.[16]

(23) Peisach, J.; Blumberg, W. E. *Arch. Biochem. Biophys.* **1974**, *165*, 691–708.

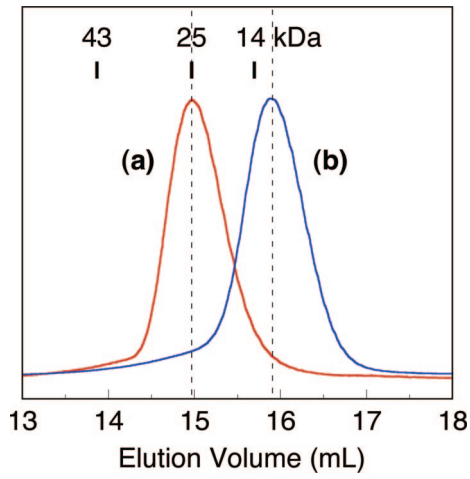

Figure 4. Elution profiles on a Superdex-75 gel filtration column (HR10/30; Pharmacia) of (a) *apo*-CopK and (b) $Cu^{I}Cu^{II}$−CopK. Conditions: each 1 mg of protein was applied in a volume of 0.21 mL; flow rate, 0.6 mL/min; potassium phosphate buffer, KPi (25 mM; pH 6.7; NaCl, 100 mM). Elution positions of molecular standards are indicated.

Table 1. Molar Mass (Da) Estimated by Sedimentation Equilibrium Analysis[a]

protein	exptl	theor[b]
Apo-CopK	16 000	8280
"Cu^{II}−CopK"[c]	15 000[d]	8343
Cu^{I}−CopK	10 000[d]	8343
Ag^{I}−CopK	9000	8387
$Cu^{I}Cu^{II}$−CopK	9000	8407

[a] All proteins (0.2 mM) in Mops buffer (10 mM, pH 7). [b] For monomer. [c] Prepared by mixing *apo*-CopK and Cu^{2+} (1:2) just prior to analysis. [d] Redox instability may affect the results in these samples slightly (see Figure S7 (Supporting Information) and eq 1).

Elution of *apo*-CopK and $Cu^{I}Cu^{II}$−CopK on a gel filtration column revealed that the former existed in solution as a multimeric protein that dissociated into monomers (theoretical molar mass, 8,280 Da) upon binding of copper (Figure 4). Sedimentation analysis on *apo*-CopK, Cu^{I}−CopK, $Cu^{I}Cu^{II}$−CopK and "Cu^{II}−CopK" at a concentration of 0.2 mM demonstrated that *apo*-CopK existed as a dimer in solution and that binding of Cu^{I}, but not the weak interaction with Cu^{2+}, led to dissociation of the dimeric *apo* form in solution (Table 1; Figure S4, Supporting Information). This is also consistent with the observed reduction in self-diffusion constants from 11.45(17) $\times$ 10^{-11} m^2 s^{-1} for *apo*-CopK to 9.44(45) $\times$ 10^{-11} m^2 s^{-1} for Cu^{I}−CopK in the NMR experiments (see below). The elution behavior of *apo*-CopK as a function of concentration on an analytical gel filtration column was consistent with a dissociation constant of $\sim 10^{-5}$ M for the *apo*-CopK dimer (Figure S5, Supporting Information). This confirms the value obtained previously by sedimentation analysis.[21]

The above observations allowed further interpretation of the changes in fluorescence intensity observed in Figure 2b during the titrations. The low affinity of dimeric *apo*-CopK for paramagnetic Cu^{2+} led to dynamic quenching of the Tyr10 fluorescence but did not induce dimer dissociation (Figure 2b(i)). The equivalent titration in the presence of NH_2OH resulted in reductive trapping of the labile Cu^{2+} as tightly bound Cu^{I} which induced dimer dissociation in solution (and a change in the environment of residue Tyr10 as signaled by the increase in emission intensity). The second equivalent of Cu^{2+} bound to a high affinity Cu^{II} binding site formed after Cu^{I} binding and dimer dissociation (Figure 2b(iii)). Titration with Cu^{+} under anaerobic conditions induced specific Cu^{I} binding with dimer dissociation but the system became air-sensitive when Cu^{I}:CopK > 1.0 and the excess labile Cu^{+} was trapped as tightly bound Cu^{II} (Figure 2b(iv)). However, experiments equivalent to titration 2b(iii) but at lower protein concentration (5−10 μM rather than 50 μM) caused much smaller changes in the fluorescence intensity until Cu:CopK > 1.0 (Figure S6a, Supporting Information). This phenomenon was observed also for equivalent titrations with Ag^{+} (Figure S6b, Supporting Information). At these lower protein concentrations, the *apo*-CopK equilibrium is displaced toward the monomer ($K_D \approx 10^{-5}$ M) whose fluorescence intensity does not respond to the binding of either Cu^{+} or Ag^{+}. However, as before, it does respond to the subsequent binding of Cu^{2+}. It is apparent that the affinity of the monomeric *apo*-CopK for Cu^{II} is also weak and that the binding cooperativity between Cu^{I} and Cu^{II} is not dependent upon dissociation of the *apo*-dimer (see quantitative analysis below).

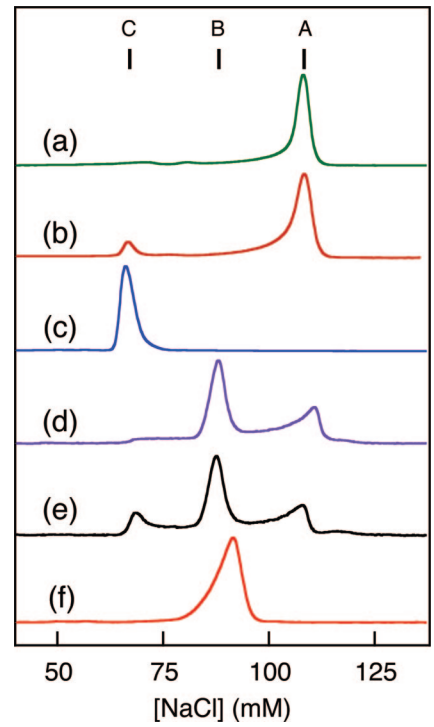

Figure 5. Elution profiles of CopK proteins ($\sim$100 μg) on a Mono-S HR5/5 cation exchange column (0.5 $\times$ 5 cm) in Mops buffer (20 mM; pH 7; NaCl gradient 0−200 mM). Protein identities (A, *apo*-CopK; B, Cu^{I}−CopK or Ag^{I}−CopK; C, $Cu^{I}Cu^{II}$−CopK or $Ag^{I}Cu^{II}$−CopK) were confirmed by protein and metal analysis (see Table 2): (a) *apo*-CopK; (b) *apo*-CopK plus 2 equiv of Cu^{2+}; (c) $Cu^{I}Cu^{II}$−CopK formed upon addition of Cu^{2+} (>2 equiv) to *apo*-CopK in the presence of NH_2OH ($\sim$20 eq) or upon addition of a mixture of *apo*-CopK and Cu^{+} (1:3). An equivalent elution profile was observed for $Ag^{I}Cu^{II}$−CopK; (d) Cu^{I}−CopK formed upon mixing *apo*-CopK (1 eq) and Cu^{+} (0.9 eq) under anaerobic conditions (the increase in absorbance starting at the elution position of the $Cu^{I}Cu^{II}$ protein and terminating at $\sim$110 mM is due to the slow oxidation of Cu^{I}−CopK to *apo*-CopK by air promoted by the affinity of the Mono-S resin for Cu^{II} ions); (e) three forms of CopK from bubbling air into Cu^{I}−CopK solution for 15 min (eq 1); (f) *apo*-CopK plus 1.1 equiv of silver acetate.

Further evidence of the binding cooperativity was provided by analytical cation exchange chromatography that was able to separate proteins of differing metal content (Figure 5).[15,17] *Apo*-CopK eluted at [NaCl] $\sim$110 mM as a trailing peak, consistent with its nature as a weakly associated dimer (Figure 5a). The presence of Cu^{2+} (2.5 eq) produced the same elution profile but with a well-defined extra component at [NaCl] $\sim$ 70 mM

Table 2. Analytical Data for CopK Proteins Eluted from a Cation Exchange Column[a]

Figure *5*	[NaCl], mM[b]	Cu^{I}, eq	Cu^{II}, eq	ESI-MS, Da[c]	assignment
a	~ 110	nd[d]	nd[d]	8280	*apo*-CopK
c	~ 70	1.1(1)	0.9(1)	8407	$Cu^{I}Cu^{II}$−CopK
d	~ 87	0.9(1)	<0.1	8343[e]	Cu^{I}−CopK
f	~ 95	nd[d]	nd[d]	8387	Ag^{I}−CopK
c	~ 70	nd[d]	1.0(1)	8451	$Ag^{I}Cu^{II}$−CopK

[a] Protein concentrations were estimated by A_{280} using ϵ_{280} = 1500, 3100 and 3000 M^{-1} cm^{-1} for Cu^{I}−, $Cu^{I}Cu^{II}$−, and $Ag^{I}Cu^{II}$−CopK, respectively. Cu^{I} and Cu^{II} concentrations were estimated spectrometrically by reagent Bcs as detailed in the Experimental Section. [b] Observed elution concentrations depended on the protein concentration, ionic strength and sample volume and so some variation was observed from experiment to experiment. [c] Detected by native ESI-MS in ammonium formate buffer (50 mM). [d] nd, not detected;. [e] Detected from a Cu^{I}−CopK sample generated *in situ* without chromatographic elution.

(Figure 5b). The proportion of this extra component increased slowly with incubation time and was about 30% of the total after 20 h (Figure S7, Supporting Information). However, inclusion of NH_2OH (10 equiv) in the reaction mixture resulted in rapid conversion to a single symmetric peak eluting at [NaCl] ≈ 70 mM (Figure 5c). Data from both copper content analysis and native ESI-MS experiments confirmed this to be $Cu^{I}Cu^{II}$−CopK (Table 2). Apparently, *apo*-CopK itself is capable of slow reduction of labile Cu^{2+} in Mops buffer to provide Cu^{+} which promotes formation of $Cu^{I}Cu^{II}$−CopK in unoxidised molecules (Figures 5b, S7, Supporting Information). Such behavior has been observed for other Met-rich proteins such as DR1885 from *Deinococcus radiodurans* and CusF from *E. coli*.[24−26] Presence of the reductant NH_2OH promoted rapid formation of $Cu^{I}Cu^{II}$−CopK whose affinity for both copper ions is sufficient to resist competition from the Mono-S resin. It is apparent that a recent interpretation of ESI-MS experiments in terms of *apo*-CopK binding two equivalents of Cu^{I} with different affinities must be modified.[21]

Incubation of *apo*-CopK protein with $[Cu^{I}(CH_3CN)_4]^{+}$ (0.9 equiv to minimize oxidation of Cu^{I}) under anaerobic conditions generated a new species which eluted at [NaCl] ≈ 87 mM on the Mono-S column (Figure 5d). Copper analysis confirmed its identity as Cu^{I}−CopK (Table 2). This form does react slowly with air to form a mixture of *apo*-CopK and $Cu^{I}Cu^{II}$−CopK (eq 1; Figure 5e). The weak affinity of *apo*-CopK for Cu^{II} ensured that the reaction did not proceed further (i.e., reaction 2 did not occur):

$$2\ Cu^{I}\text{−CopK} \xrightarrow{O_2} \textit{apo}\text{-CopK} + Cu^{I}Cu^{II}\text{−CopK} \qquad (1)$$

$$\textit{apo}\text{-CopK} + Cu^{I}Cu^{II}\text{-CopK} \xrightarrow{O_2} 2\ Cu^{II}\text{-CopK} \qquad (2)$$

The absorbance increase in Figure 5d commencing at [NaCl] ≈ 70 mM arises from the product $Cu^{I}Cu^{II}$−CopK of reaction 1, initiated by the affinity of the Mono-S resin for copper cations.

We and others have demonstrated that the periplasmic copper resistance proteins PcoC from *E. coli* and CopC from *P. syringae* feature separate binding sites specific for Cu^{I} and Cu^{II},

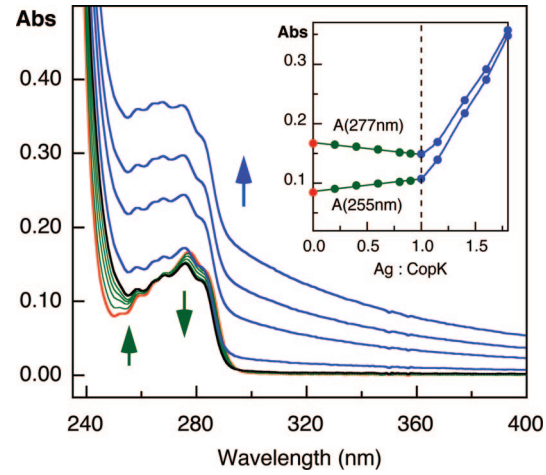

Figure 6. Changes in the solution spectrum of *apo*-CopK (100 μM) in Mops buffer (20 mM; pH 7) upon titration with silver acetate solution. (Inset) Plots of A_{255} and A_{277} versus Ag:CopK. The spectral changes at Ag: CopK < 1 report Ag^{I} binding, rather than *apo*-CopK dissociation. Equivalent titration with monomeric *apo*-PcoC induced similar spectral changes in the UV region.

respectively.[15,17,27] The Cu^{I} forms were air-sensitive and oxidized readily to the stable Cu^{II} forms in two-step processes equivalent to eqs 1 and 2 above (eq 3):

$$2Cu^{I}\text{−CopC} \xrightarrow{O_2} \textit{apo}\text{-CopC} + Cu^{I}Cu^{II}\text{−CopC} \xrightarrow{O_2} 2Cu^{II}\text{−CopC} \qquad (3)$$

However, the chemistry of CopK is distinctly different. The affinity of *apo*-CopK for Cu^{II} was enhanced only upon binding of Cu^{I} and this effect drove reaction 1, but prevented further reaction 2 even in an air-saturated solution (Figure S8, Supporting Information).

Apo-CopK also binds Ag^{+}. Titration of *apo*-CopK (100 μM) in Mops buffer (20 mM; pH 7) with silver acetate solution induced minor but distinct spectral changes in the UV region with an isosbestic point around 264 nm and a clear end point at Ag^{I}:CopK = 1 (Figure 6). The absorbance ratio A_{255}/A_{277} changed from 0.49 for *apo*-CopK to 0.72 for Ag^{I}−CopK. However, further addition of Ag^{+} caused precipitation, as indicated by the shifting baseline. A linear increase in fluorescence intensity was also observed for equivalent titrations, consistent with conversion of *apo*-CopK dimer to Ag^{I}−CopK monomer in solution (Figure S6b(i), Supporting Information). This was confirmed by sedimentation analysis (Table 1).

Air-stable Ag^{I}−CopK was robust enough to survive elution from the Mono-S column, albeit as a trailing peak, presumably due to competition with the Mono-S resin for Ag^{+} (Figure 5f; Table 2). However, addition of Cu^{2+} to Ag^{I}−CopK produced stable $Ag^{I}Cu^{II}$−CopK that eluted cleanly as a symmetrical peak at the same NaCl concentration as that for the $Cu^{I}Cu^{II}$−CopK form (Figure 5c; Table 2). It appeared that binding of both Ag^{I} and Cu^{II} by CopK had enhanced the binding affinities for both

(24) Banci, L.; Bertini, I.; Ciofi-Baffoni, S.; Katsari, E.; Katsaros, N.; Kubicek, K.; Mangani, S. *Proc. Natl. Acad. Sci. U.S.A.* **2005**, *102*, 3994–3999.
(25) Xue, Y.; Davis, A. V.; Balakrishnan, G.; Stasser, J. P.; Staehlin, B. M.; Focia, P.; Spiro, T. G.; Penner-Hahn, J. E.; O'Halloran, T. V. *Nat. Chem. Biol.* **2008**, *4*, 107–109.
(26) Consistent with CopK protein itself as a slow reductant for Cu^{2+}, in our analysis of Cu^{I} and Cu^{II} content by Bcs (see Experimental Section), we found that removal of Cu^{I} by Bcs from $Cu^{I}Cu^{II}$−CopK released Cu^{2+} that was reduced slowly to Cu^{I}. Thus, the Cu^{I} content detected with Bcs increased slightly with incubation time in the expense of Cu^{II} conent while the total copper content remained unchanged.
(27) Arnesano, F.; Banci, L.; Bertini, I.; Mangani, S.; Thompsett, A. R. *Proc. Natl. Acad. Sci. U.S.A.* **2003**, *100*, 3814–3819.

Table 3. Estimation of $K_D(Cu^I-CopK)$ by Competition for Cu^I between CopK and Bca in the Absence and Presence of Cu^{2+}[a,b]

expt	solution conditions	$[CopK]_{tot}$ μM	A_{562}	A_{358}	$[Cu^I(Bca)_2]^{3-}$ μM[c]	$[Cu^I-P]$ μM[d]	$K_D(Cu^I-P)$ M[e]	increase in apparent $K_D(Cu^I-P)$ [f]
1	Asc, 500 μM (no Cu^{2+})	0	0.114	0.621	14.5	0		
		100	0.104	0.562	13.1	1.3	1.8×10^{-11}	
		200	0.099	0.536	12.5	1.9	2.1×10^{-11}	
		300	0.095	0.513	12.0	2.4	2.1×10^{-11}	
		400	0.091	0.490	11.4	3.0	2.0×10^{-11}	
2	$[Cu^{2+}] = [CopK]$ (no Asc)	0	0.114	0.621	14.5	0		
		12.5	0.079	0.427	10.0	4.5	1.7×10^{-13}	120
		25	0.065	0.347	8.1	6.4	1.8×10^{-13}	110
		50	0.048	0.257	6.0	8.5	1.7×10^{-13}	120
		100	0.034	0.186	4.3	10.2	1.8×10^{-13}	110

[a] In Tris/Mes buffer (20 mM; pH 8; NaCl, 100 mM) under anaerobic conditions. [b] Total Bca concentration in all equilibrium solutions was 45 μM. [c] Calculated based on the absorbances at 358 nm with $\epsilon = 42\,900$ M^{-1} cm^{-1}; essentially identical results can be calculated from the absorbances at 562 nm with $\epsilon = 7900$ M^{-1} cm^{-1}. [d] Equal to decrease in $[Cu^I(Bca)_2]^{3-}$ concentration relative to the same solution without CopK protein. [e] Calculated from eq 5 for expt 1 and eq 7 for expts 2 and 3. [f] Relative to an average $K_D(Cu^I-P) = 2.0 \times 10^{-11}$ M for *apo*-CopK.

metal ions. Addition of other metal ions (Ni^{2+}, Co^{2+}, Zn^{2+}, Cd^{2+}, Hg^{2+}) to Ag^I-CopK did not induce this effect and Ag^I-CopK only was recovered after elution from the Mono-S column.

In summary, *apo*-CopK exists in solution as a weakly associated dimer[21] with weak affinity for Cu^{II} but with high affinity for Cu^I and Ag^I. Binding of the latter ions induces structural changes in solution that include dissociation of the *apo*-CopK dimer and formation of Cu^I-CopK and Ag^I-CopK whose affinities for Cu^{II} were enhanced considerably and specifically. Both $Cu^ICu^{II}-CopK$ and $Ag^ICu^{II}-CopK$ were stable in air and eluted cleanly as well-defined peaks from the cation exchange column.

Binding Cooperativity between Cu^I and Cu^{II}. Cu^I Binding Affinities. *Apo*-CopK binds Cu^+ to generate moderately air-sensitive Cu^I-CopK. Competition with the chromophoric Cu^I ligand bicinchoninic anion (Bca) under anaerobic conditions allowed quantitative estimation of the Cu^I affinity (see Experimental Section for details):[15]

$$[Cu^I(Bca)_2]^{3-} + apo\text{-CopK} \rightleftharpoons Cu^I-CopK + 2Bca^{2-} \quad K_{ex4} \quad (4)$$

$$K_{D4}(Cu^I) = (\beta_2 \times K_{ex4})^{-1} = \beta_2^{-1} \times \frac{[Cu^I(Bca)_2][CopK]}{[Cu^I-CopK][Bca]^2} \quad (5)$$

The overall formation constant β_2 for $[Cu^I(Bca)_2]^{3-}$ has been determined recently by two independent approaches providing estimates which differ by 2.5 orders of magnitude ($10^{17.2}$ versus $10^{14.7}$ M^{-2}).[28,29] The former value was estimated by indirect competition for Cu^I between ligands Bca and bathocupröine disulfonate (Bcs; $\beta_2 = 10^{19.8}$ M^{-2}) mediated separately by three *apo* proteins that bind Cu^I with different affinities (Atx1, nA-PcoC and C42S-rubredoxin).[28,30] This value was confirmed by the equivalent competition mediated by *Bacillus subtilis* CopZ protein.[31] The second estimate was obtained by isothermal titration calorimetry via titration of a Cu^+ solution with Bca.[29] The Cu^+ solution was generated by reduction of Cu^{2+} with ascorbate (Asc) in NaCl (200 mM) which stabilizes Cu^+ as $[Cu^ICl_n]^{(1-n)-}$. Titration with Bca would involve a conversion of these species to $[Cu^I(Bca)_2]^{3-}$, diminishing the observed heat

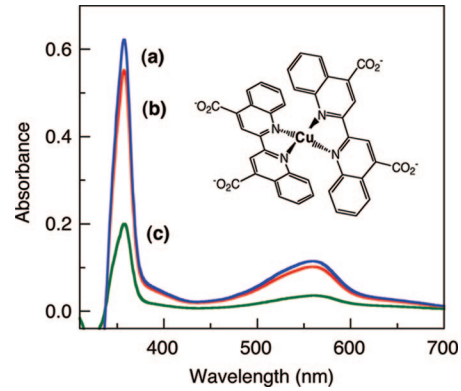

Figure 7. Solution absorbance spectra in Tris/Mes buffer (20 mM; pH 8; NaCl, 100 mM). (a) Mixture of $[Cu^I(CH_3CN)_4]^+$ (14.5 μM), Bca (45 μM) and Asc (500 μM) (blue trace; Table 3); substitution of Asc with Cu^{2+} (100 μM) did not change the spectrum; (b) after addition of *apo*-CopK (100 μM) into solution (a) (red trace); (c) as for (b) but with Cu^{2+} (100 μM) instead of Asc (green trace). (Inset) Structure of $[Cu^I(Bca)_2]^{3-}$.

release. Nevertheless, the β_2 values obtained from the two different approaches agree reasonably well. In this work, we adopted a value of $\beta_2 = 10^{17.2}$ M^{-2}. A series of competition experiments in the absence of Cu^{2+} (eq 4) provided $K_D(Cu^I) = 2.0(2) \times 10^{-11}$ M for *apo*-CopK according to eq 5 (Table 3, expt 1).

Addition of Cu^{2+} into a solution with composition similar to that in expt 1 with $[CopK]_{total} = 100$ μM but in the absence of a reductant decreased the absorbance arising from $[Cu^I(Bca)_2]^{3-}$ considerably (compare Figure 7b and c). The equivalent experiment on a control solution lacking CopK caused no detectable change. While the addition of Cu^{2+} did not affect the sensitivity of the Bca probe for Cu^+, its presence has affected the affinity of CopK for Cu^I:

$$[Cu^I(Bca)_2]^{3-} + "Cu^{II}-CopK" \rightleftharpoons Cu^ICu^{II}-CopK + 2Bca^{2-} \quad K_{ex6} \quad (6)$$

$$K_{D6}(Cu^I) = (\beta_2 \times K_{ex6})^{-1} = \beta_2^{-1} \times \frac{[Cu^I(Bca)_2]["Cu^{II}\text{- CopK"}]}{[Cu^ICu^{II}\text{- CopK}][Bca]^2} \quad (7)$$

where "$Cu^{II}-CopK$" defines the total CopK species that are not associated with Cu^I. Accordingly, the apparent affinity of "$Cu^{II}-CopK$" for Cu^I ($K_{D6}(Cu^I)$) can be defined and calculated according to eq 7 as detailed in the Experimental Section. The binding cooperativity between Cu^I and Cu^{II} ensured that $Cu^ICu^{II}-CopK$ was the dominant Cu^I-containing CopK species

(28) Xiao, Z.; Donnelly, P. S.; Zimmermann, M.; Wedd, A. G. *Inorg. Chem.* **2008**, *47*, 4338–4347.
(29) Yatsunyk, L. A.; Rosenzweig, A. C. *J. Biol. Chem.* **2007**, *282*, 8622–8631.
(30) Xiao, Z.; Loughlin, F.; George, G. N.; Howlett, G. J.; Wedd, A. G. *J. Am. Chem. Soc.* **2004**, *126*, 3081–3090.
(31) Zhou, L.; Singleton, C.; Le Brun, N. E. *Biochem. J.* **2008**, *413*, 459–465.

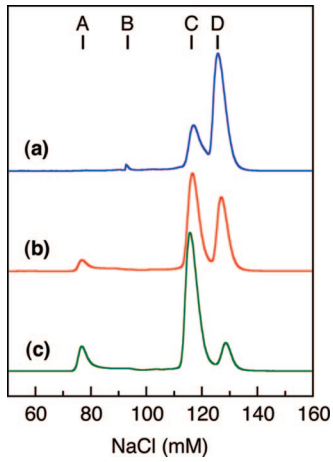

Figure 8. Elution profiles under the conditions of Figure 5 demonstrating competition for Cu^{I} between CopK and Cu^{II}−PcoC in the absence and presence of Cu^{2+}: (a) *apo*-CopK:$Cu^{I}Cu^{II}$−PcoC = 1:1. (b) Cu^{2+}:*apo*-CopK:$Cu^{I}Cu^{II}$−PcoC = 1:1:1. The chromatogram for the reaction with Cu^{2+}:$Cu^{I}Cu^{II}$−CopK:Cu^{II}−PcoC = 1:1:1 was indistinguishable. (c) Cu^{2+}:*apo*-CopK:$Cu^{I}Cu^{II}$−PcoC = 2:2:1. The elution position of each protein is labeled: A, $Cu^{I}Cu^{II}$−CopK; B, Cu^{I}−CopK; C, *apo*-CopK or Cu^{II}−PcoC; D, $Cu^{I}Cu^{II}$−PcoC. Protein identities were confirmed by ESI-MS and copper content analysis. Note: the ε_{280} value for $Cu^{I}Cu^{II}$−PcoC is approximately 5 times that for $Cu^{I}Cu^{II}$−CopK.

and that there is negligible contribution from Cu^{I}−CopK under the conditions $[Cu^{2+}]_{total} \geq [Cu^{+}]_{total}$. For those experiments in which $[Cu^{2+}]_{total} = [CopK]_{total}$, $K_{D6}(Cu^{I})$ increased by 2 orders of magnitude relative to $K_{D4}(Cu^{I})$ in the absence of Cu^{2+} (Table 3, expt 2). It can be concluded that CopK features a strong Cu^{I} binding site whose affinity for Cu^{I} is enhanced further when Cu^{2+} is available for co-binding.

This conclusion was confirmed by direct competition for Cu^{I} between CopK and the Cu^{I} binding protein Cu^{II}−PcoC ($K_{D}(Cu^{I}) \approx 10^{-13}$ M).[15,32] A solution containing equimolar concentrations of *apo*-CopK and $Cu^{I}Cu^{II}$−PcoC in Mops buffer (20 mM, pH 7) was incubated for 30 min and subjected to quantitative separation by cation exchange chromatography. Very little Cu^{I} was transferred from $Cu^{I}Cu^{II}$−PcoC to *apo*-CopK (reaction 8; Figure 8a). However, addition of one equiv of Cu^{2+} to the solution led to significant transfer of Cu^{I} from $Cu^{I}Cu^{II}$−PcoC to produce $Cu^{I}Cu^{II}$−CopK protein (eq 9; Figure 8b: note that the elution positions of *apo*-CopK and Cu^{II}−PcoC overlap and that the ε_{280} value for $Cu^{I}Cu^{II}$−PcoC is approximately 5 times that for $Cu^{I}Cu^{II}$−CopK). Doubling the concentration of both Cu^{2+} and *apo*-CopK shifted the position of equilibrium to the right (eq 9; Figure 8c):

$$\textit{apo}\text{-CopK} + Cu^{I}Cu^{II}\text{−PcoC} \leftrightarrows Cu^{I}\text{−CopK} + Cu^{II}\text{−PcoC} \quad (8)$$

$$\textit{apo}\text{-CopK} + Cu^{I}Cu^{II}\text{−PcoC} + Cu^{2+} \rightleftharpoons Cu^{I}Cu^{II}\text{−CopK} + Cu^{II}\text{−PcoC} \quad (9)$$

An elution profile essentially indistinguishable from that of Figure 8b was produced from the reverse reaction starting with equimolar concentrations of $Cu^{I}Cu^{II}$−CopK and Cu^{II}−PcoC. These experiments demonstrate that the affinity of *apo*-CopK for Cu^{I} is weaker than that of Cu^{II}−PcoC but that when Cu^{2+} is available, their affinities for Cu^{I} are comparable.[32]

(32) As a control, equivalent competition experiments were carried out for protein PcoC that binds both Cu^{I} and Cu^{II} at two separate sites with high affinities. The affinity of Cu^{II}-PcoC for Cu^{I} was very similar to that of *apo*-PcoC ($\sim 2 \times 10^{-13}$ M) and was independent on the ratio of $[Cu^{II}]/[PcoC]$ in the solution.

Ag^{I} Binding Affinities. The relative affinities of CopK for Cu^{I} and Ag^{I} were compared by competitive binding experiments in the absence and presence of Cu^{2+}. Titration of 0.4 eq of Cu^{+} into a solution of Ag^{I}−CopK (100 μM) under anaerobic conditions induced an absorbance increase at 260 nm, signaling that the Ag^{I} in Ag^{I}−CopK was replaced by the added Cu^{+} (cf, Figures S3 (Supporting Information) and 6):

$$Ag^{I}\text{−CopK} + Cu^{+} \rightarrow Cu^{I}\text{−CopK} + Ag^{+} \quad (10)$$

Further addition of 0.2 equivalent of Cu^{+} released more Ag^{+} which caused protein precipitation (see Figure 6). The equivalent titration of Cu^{+} into an anaerobic solution of $Ag^{I}Cu^{II}$−CopK produced similar results. In separate experiments, Cu^{+} (1.1 equiv) followed by equimolar Ag^{+} was added to *apo*-CopK solution, followed by the addition of Cu^{2+} (1.5 equiv). A second system differing only in the order of addition of Cu^{+} and Ag^{+} was also prepared. The total protein components were recovered as a single elution peak on the Mono-S column (Figure 5c). Analysis of copper contents by Bcs produced a consistent ratio of Cu^{I}:Cu^{II} = 0.8:1.0 for both protein solutions while a control of $Cu^{I}Cu^{II}$−CopK gave a ratio of Cu^{I}:Cu^{II} = 1.1:0.9 (Table 2). These experiments demonstrate that the affinity of CopK for Ag^{I} is weaker than that for Cu^{I}, both in the absence and in the presence of Cu^{2+}.

Cu^{II} Binding Affinities. As demonstrated above, *apo*-CopK exhibits weak affinity for Cu^{II} ($K_{D} > 10^{-6}$ M; Figures 2b(i) and S3, Supporting Information) and the Cu^{II} form cannot survive a gel filtration column. However, addition of Cu^{+} or Ag^{+} enhances the affinity for Cu^{II} dramatically and both $Cu^{I}Cu^{II}$−CopK and $Ag^{I}Cu^{II}$−CopK were eluted cleanly from the Mono-S cation exchange column (Figure 5c; Table 2). Thus a quantitative estimation of $K_{D}(Cu^{II})$ for Cu^{I}−CopK requires competition with suitable Cu^{II} ligands of known binding affinities. However, the Tyr 10 fluorescence probe of CopK is not suitable for monitoring the variation of Cu^{II} occupancy on CopK due to the dependence of its intensity upon the monomer−dimer equilibrium of *apo*-CopK and the dynamic quenching caused by paramagnetic Cu^{II} species in solution (see Figures 2 and S6, Supporting Information). We have determined previously the Cu^{II} affinities of CopC from *P. syringae* and PcoC from *E. coli*.[15,17] Both proteins fluoresce intensely with an emission maximum at 324 nm due to the presence of a single Trp residue in each protein molecule. Cu^{II} binding quenched the fluorescence intensities linearly until one equivalent of Cu^{II} was bound, providing the necessary probe to monitor the variation of Cu^{II} occupancies on both proteins. This favorable property was applied in the present case to competition for Cu^{2+} between Cu^{I}−CopK and a CopC triple variant M40L/M43L/H48F-CopC. The mutations disable the Cu^{I} site. This protein is designated as ■□-CopC where ■ and □ indicate the disabled Cu^{I} site and the empty Cu^{II} site, respectively.[17] The competition for Cu^{2+} can be represented by:

$$■Cu^{II}\text{−CopC} + Cu^{I}\text{−CopK} \rightleftharpoons ■\,□\text{−CopC} + Cu^{I}Cu^{II}\text{−CopK} \quad (11)$$

$$\frac{K_{D}(■Cu^{II})}{K_{D}(Cu^{II})} = \left(\frac{[■\,□\text{−CopC}]_{total}}{[■Cu^{II} - CopC]} - 1\right) \Big/ \left(\frac{[Cu^{I} - CopK]_{total}}{[Cu^{I}Cu^{II} - CopK]} - 1\right) \quad (12)$$

As detailed in the Experimental Section, the corrected change in fluorescence intensity ΔF_{obs} can quantify the amount of Cu^{II}

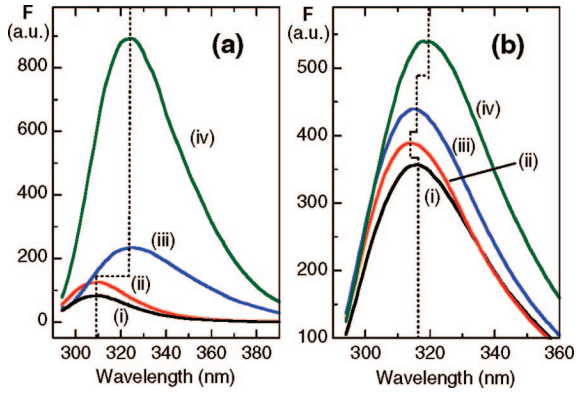

Figure 9. (a) Fluorescence spectra for proteins (10 μM) recorded under the same conditions: (i) $Cu^{I}Cu^{II}$−CopK; (ii) *apo*-CopK; (iii) ■Cu^{II}−CopC; (iv) ■□-CopC. (b) Determination of $K_D(Cu^{II})$ for Cu^{I}−CopK by competition for Cu^{II} with ■□-CopC in Mops (20 mM; pH 7.0; Na_2SO_4, 50 mM): (i) initial solution containing Cu^{II} (4.5 μM), ■□-CopC (5.0 μM) and *apo*-CopK (20 μM) (the total intensity at 320 nm was estimated to be contributed 45% from CopC and 55% from CopK); (ii) after addition of Ag^+ (18 μM) into solution (i); (iii) after addition of Cu^+ (18 μM) into solution (i); (iv) after addition of Edta (10 equiv) into solution (i).

transferred from ■Cu^{II}−CopC to Cu^{I}−CopK in reaction 11. To correctly assess background, the air-sensitive Cu^{II} competitor Cu^{I}−CopK was generated *in situ* from *apo*-CopK by reaction with substoichiometric amounts of $[Cu(CH_3CN)_4]^+$ with the background contribution from *apo*-CopK dimer dissociation $\Delta F_{D\text{-}M}$ estimated from the equivalent experiments with Ag^+. The advantages of this competing system include: (i) ΔF_{CopC} at 320 nm is 20 times more sensitive than ΔF_{CopK} for the Cu^{II} transfer in reaction 11 (see Figure 9a) and thus the estimation can be based on the more reliable CopC probe ΔF_{CopC} with background $\Delta F_{D\text{-}M}$ correction; (ii) the Cu^{II} transfer between CopK and CopC proteins was fast (<5 min), minimizing the possibility of Cu^{I} oxidation.

A set of data from three separate experiments (one is displayed in Figure 9b) allowed the amount of Cu^{II} transferred in reaction 11 to be defined and thus $K_D(Cu^{II})$ for Cu^{I}−CopK to be calculated according to eq 12 (see Experimental Section for details). A series of experiments with varying concentrations and stoichiometries of the competing components led to a consistent estimate of $K_D(Cu^{II}) = 2.5(5) \times 10^{-12}$ M for Cu^{I}−CopK (Table 4). This is the first report of quantitative estimation of $K_D(Cu^{II})$ for an air-sensitive Cu^{I}-protein.

Three conclusions about $K_D(Cu^{II})$ can be drawn from the data in Table 4: (i) *apo*-CopK does not compete with ■□-CopC for Cu^{II} (note ΔF_{obs} in expts 2, 4 and 6, 8), consistent with $K_D(Cu^{II}) > 10^{-6}$ M for *apo*-CopK; (ii) Cu^{I} binding has increased the affinity for Cu^{II} by at least 6 orders of magnitude; (iii) the observed binding cooperativity is not dependent on the solution state of *apo*-CopK (dimer or monomer).

X-Ray Crystallography. Crystal Structures of apo-CopK and Cu^{I}−CopK. Crystals of Cu^{I}−CopK were grown from a preparation of $Cu^{I}Cu^{II}$−CopK, with PEG MME 2000 and KSCN in an unbuffered crystallization solution. Highly redundant data were collected in space group $P2_12_12$ to 1.55 Å resolution, which allowed experimental single wavelength anomalous dispersion (SAD) phases to be calculated from eight sulfur positions per asymmetric unit. Early in the refinement procedure, the position of a single Cu atom per asymmetric unit was identified in difference Fourier electron density maps. This assignment was confirmed in anomalous difference Fourier electron density maps, calculated using X-ray diffraction data collected at energies either side of the Cu K-edge (8.996 and 8.960 keV, referred to as 'peak' and 'remote' data sets, respectively). A significant peak (22 σ) was observed coincident with the position of the Cu atom in the map calculated from the 'peak' data, but not in the map from the 'remote' data (data not shown). Subsequent analysis of its coordination geometry indicated it to be a Cu^{I} atom (see below). Therefore, although $Cu^{I}Cu^{II}$−CopK was submitted to crystallization trials, the crystals contained Cu^{I}−CopK only. The model of Cu^{I}−CopK includes residues 1−66, a single Cu^{I} atom, two SCN^- ions (originating from the crystallization solution) and 64 water molecules. *Apo*-CopK crystallized in space group *C*2 and diffraction data were collected to 2.2 Å resolution. The structure was solved by molecular replacement using the refined coordinates of Cu^{I}−CopK. The statistics for both the Cu^{I}- and *apo*-CopK structures are given in Table S1, Supporting Information. The structures both refined to *R*-factors <25% and have excellent stereochemistry. No ordered electron density was observed for residues 67−74 in each structure and these residues have accordingly been omitted from the models. A ribbon representation of Cu^{I}−CopK is presented in Figure 10. The coordinates of the Cu^{I}−CopK and *apo*-CopK structures have been deposited with the Protein Data Bank with accession codes 3dso and 3dsp, respectively.

There is a single molecule in the asymmetric unit of each structure. They are conformationally identical, with two antiparallel β-sheets arranged in a sandwich-like structure (Figures 10a, b). The two sheets are formed by residues 6−11, 17−21, 26−29, 35−36 (strands β1-β4) and residues 44−45, 51−55 and 58−61 (β5-β7), respectively (see Figure 1). There are a total of five hydrogen-bonding interactions between the two β-sheets: four that involve residues on loops linking strands β1-β2 and β5-β6 and one involving residues on the loops linking strands β2-β3 and β6-β7 (Table 5). Significantly, for Cu^{I}−CopK, the coordination of the single Cu^{I} atom provides a sixth bridging interaction between the two β-sheets. The Cu^{I} atom is ligated by Met residues 26, 38 and 54, with Met S^{δ}-Cu^{I} distances between 2.28−2.35(6) Å. A fourth ligand was modeled as an isothiocyanate ion (SCN-Cu^{I} = 2.21(6) Å), originating from the crystallization solution. The coordination geometry is approximately tetrahedral with an average Met S^{δ}/N(SCN^-) > Cu^{I} > Met S^{δ}/N(SCN^-) angle of 115° (Figure 10d). The S^{δ} atoms of the other three Met residues 28, 36 and 44 lie 6.4, 10.4 and 7.4 Å, respectively, from the Cu^{I} atom. Without a major structural change, these Met residues are too far away to be Cu^{I} ligands. When $Cu^{I}Cu^{II}$−CopK was crystallized in the absence of SCN^-, the structure of the Cu^{I} binding site was essentially conserved, apart from the absence of SCN^-.[33]

The crystal structures of *apo*-CopK and Cu^{I}−CopK superpose well with a rmsd of 0.55 Å. This is comparable to the combined coordinate errors of the two structures and indicates no substantial structural change upon Cu^{I} coordination for the crystalline dimeric form. These structures are very similar to the dimeric *apo*-CopK-NMR structure that exists in solution also as a dimer (Figure 10c).[21] When the best representative conformer from the NMR ensemble (PDB code 2k0q) is superposed on the crystal structures of *apo*-CopK and Cu^{I}−CopK, the rmsd values are 0.98 and 1.05 Å, respectively. Again, these values are within the combined coordinate errors of the respective models and confirm similar solution and crystalline molecular states for these proteins in their dimeric

(33) Ash, M.-R.; Maher, M. J. Unpublished results.

Table 4. Determination of $K_D(Cu^{II})$ for Cu^I−CopK by Competition for Cu^{II} with a CopC Triple Variant (■□-CopC) in Mops Buffer (20 mM; pH 7.0; 50 mM Na_2SO_4)

	precompetition			competition						
expt	$[Cu^{II}_{0.9}$-CopC] μM	[*apo*-CopK] μM	F_{pre} (320)	+ Cu^+ μM	F_{comp} (320)	ΔF_{obs}[a]	ΔF_{CopC}[a]	$\Delta F_{CopC}/\Delta F_{0.9}$[a]	$[Cu^ICu^{II}$−CopK] μM[c]	$K_D(Cu^{II})$[d] 10^{-12} M
1	5	20	346	−	539[b]	193	193	1.0	−	−
2	5	20	348	9.0	385	37	33	0.17	0.77	2.3
3	5	20	348	18	422	74	55	0.29	1.3	1.7
4	5	10	290	9.0	327	37	35	0.18	0.81	2.0
5	10	40	595	−	955[b]	360	360	1.0	−	−
6	10	40	595	18	671	76	51	0.14	1.3	3.2
7	10	40	595	36	755	160	84	0.23	2.1	2.6
8	10	20	475	18	547	72	53	0.15	1.3	3.0

[a] $\Delta F_{obs} = F_{comp} - F_{pre}$; $\Delta F_{CopC} = \Delta F_{obs} - \Delta F_{D-M}$ where ΔF_{D-M} was the increase in F due to conversion of *apo*-CopK dimer to monomer upon addition of equal amount of Ag^+ into the same precompetition solution (see Figure 6); $\Delta F_{0.9}$ is the increase in F after the bound Cu^{II} (0.9 equiv) in CopC was fully removed by Edta (10 equiv). [b] Fluorescence intensity after addition of Edta (10 equiv) to remove the bound Cu^{II} (0.9 equiv) from Cu^{II}−CopC. [c] Cu^{II} transferred from Cu^{II}−CopC to Cu^I−CopK, equal to $[CopC]_{total} \times (\Delta F_{CopC}/\Delta F_{0.9}) \times 0.9$. [d] Calculated according to eq 12 with $K_D(Cu^{II}$−CopC$) = 7.2 \times 10^{-14}$ M[17] and other required terms calculated on mass balance from the experimental data of $[Cu^ICu^{II}$−CopK].

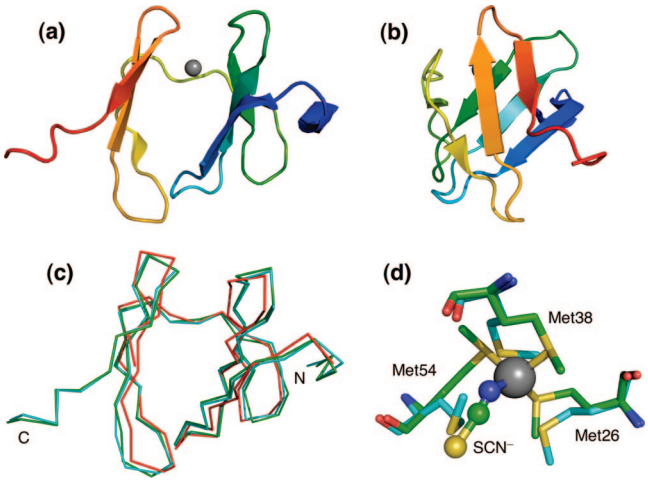

Figure 10. Crystal structure of Cu^I−CopK. (a) Structure is represented as a Cα trace with secondary structure indicated. The chain is colored from blue at the N-terminus to red at the C-terminus. The Cu^I atom is shown as a gray sphere. (b) Different view of (a) after 90° rotation around the vertical axis. (c) Superposition of the backbone structures of Cu^I−CopK (green), *apo*-CopK (cyan, by X-ray; red, by NMR[21]). (d) Superposition of the Cu binding sites of Cu^I−CopK (green carbon atoms) and *apo*-CopK (cyan carbon atoms). For both structures, nitrogen atoms are colored blue; sulfur, yellow; and oxygen, red. The Cu atom is represented as a gray sphere. The SCN^- ion as the fourth Cu^I ligand is shown in a ball-and-stick representation.

Table 5. Intra- and Inter-Molecular Hydrogen-Bonding Interactions in *apo*-CopK and Cu^I−CopK

Distance	*apo*-CopK[a]	Cu^I−CopK[a]
Intramolecular hydrogen-bonding interactions between β-sheets (Å)		
11 Asp O − 47 Arg N	2.63	2.80
13 Gln N − 45 Glu O	3.03	2.86
13 Gln $N^{\epsilon 2}$ − 45 Glu $O^{\epsilon 2}$	3.32	2.89
13 Gln $N^{\epsilon 2}$ − 46 Thr O	3.07	3.30
24 Gly O − 57 Asn $N^{\delta 2}$	4.46	3.10
Intermolecular hydrogen-bonding interactions between CopK monomers (Å)		
8 Lys N^{ζ} − 63 Asp $O^{\delta 2}$	3.62	2.78
10 Tyr OH − 63 Asp $O^{\delta 2}$	2.46	2.55
41 Gly O − 55 Lys N^{ζ}	2.72	3.14
51 Lys N^{ζ} − 58 Glu $O^{\epsilon 1}$	2.58	−
51 Lys N^{ζ} − 58 Glu $O^{\epsilon 2}$	3.46	−
55 Lys N^{ζ} − 41 Gly O	2.72	3.14
58 Glu $O^{\epsilon 1}$ − 51 Lys N^{ζ}	2.58	−
58 Glu $O^{\epsilon 2}$ − 51 Lys N^{ζ}	3.46	−
59 Ile O − 63 Asp N	2.92	2.84
61 Arg N − 61 Arg O	2.64	2.83
61 Arg O − 61 Arg N	2.64	2.83
63 Asp N − 59 Ile O	2.92	2.84
63 Asp $O^{\delta 2}$ − 8 Lys N^{ζ}	3.62	2.78
63 Asp $O^{\delta 2}$ − 10 Tyr OH	2.46	2.58

[a] For both *apo*- and Cu^I−CopK structures, the dimer is generated by the application of crystallographic symmetry operations. The dimer can be described as A/A*, where A is the molecule in the asymmetric unit, and A* is generated by -*x*, *y*, *z* and -*x*+1, -*y*, *z* for *apo*- and Cu^I−CopK structures, respectively.

forms. The major differences between the *apo*-CopK, Cu^I−CopK and *apo*-CopK-NMR structures are in the conformations of side chains. As expected, a number of surface-exposed residues have different conformations in the three structures. Importantly, those of the Cu^I ligands Met26, Met38 and Met54 depend upon the presence of the Cu^I ion (Figure 10d), with the largest shifts being for Met38 and Met54. However, as reflected in the superpositions described above, these rearrangements have little impact on the structure of the protein main chain.

Application of crystallographic symmetry operations to both the *apo*-CopK and Cu^I−CopK structures demonstrated that each crystal is composed of dimers, where the monomers interact through their C-terminal β-strands (Figure 11). About 16% of the solvent accessible area of each monomer is buried upon dimer formation (818 $Å^2$ from 4822 $Å^2$ for *apo*-CopK and 793 $Å^2$ from 4826 $Å^2$ for Cu^I−CopK). The intermolecular interactions are mediated by a significant number of specific hydrogen bonds (Table 5). Notably, the fluorescent residue Tyr10 is also found at the dimer interface and participates in an intermolecular hydrogen-bonding interaction with Asp63. Dissociation of the dimer would be expected to influence the local environment of Tyr10 considerably. Indeed, binding by either Cu^I or Ag^I induced significant changes in both its NMR chemical shift and its fluorescence intensity (Figures 2, S6 (Supporting Information), 12a).

Solution Properties of CopK Proteins Characterized by NMR. Solution NMR spectroscopy was used to probe the nature of the species present after addition of metal ions to CopK solutions. Resonance assignments of *apo*-CopK, Cu^ICu^{II}−CopK and the backbone assignments of Cu^I−CopK and Ag^I−CopK were determined using a standard array of heteronuclear multidimensional NMR techniques.[34] Well-dispersed $^1H-^{15}N$ HSQC spectra were observed in each case (Figure 12), indicating that they are all folded species in solution.[21] Titration of *apo*-CopK with $[Cu^I(CD_3CN)_4]^+$ under anaerobic conditions led

(34) Sattler, M.; Schleucher, J.; Griesinger, C. *Prog. Nucl. Magn. Reson. Spectrosc.* **1999**, *34*, 93–158.

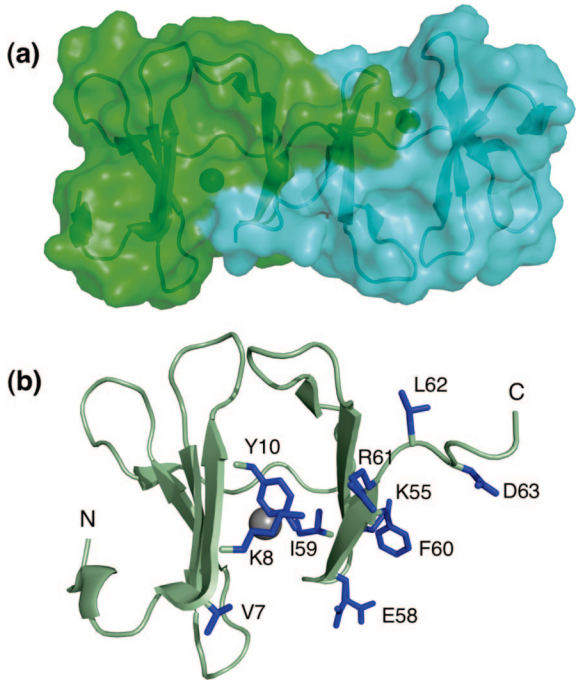

Figure 11. (a) Crystal structure of the Cu^{I}−CopK dimer. The dimer A/A* is generated by the symmetry operation $-x+1, -y, z$. One monomer is shown in green, the other in cyan. The transparent surfaces of each monomer are superposed on a trace of their Cα positions. The secondary structural elements are indicated. The Cu atoms are shown as gray spheres. (b) CopK molecule in the dimer showing residues (in stick representation) in the dimer interface that experience resonance broadening or are missing in the $^{1}H-^{15}N$ heteronuclear single quantum coherence (HSQC) spectrum when compared to that of *apo*-CopK. This suggests a shift of the dimer-monomer equilibrium toward dissociation upon Cu^{I} binding in solution (see Figure 12a).

to the appearance of a new set of resonances in the HSQC spectra (green contours) at the expense of those of *apo*-CopK (black contours). The latter resonances disappeared completely after addition of one equivalent of $[Cu^{I}(CD_3CN)_4]^{+}$. The observed self-diffusion constant also decreased from 11.45(17) $\times$ 10^{-11} m^2 s^{-1} to 9.44(45) $\times$ 10^{-11} m^2 s^{-1}, indicating a reduction in the molecular size after addition of Cu^{I}. Collectively, these results indicate tight binding of Cu^{I}, consistent with the estimated $K_D = 2.0 \times 10^{-11}$ M (Table 3) and conversion of dimeric *apo*-CopK to monomeric Cu^{I}−CopK (Table 1).

When compared to *apo*-CopK, a number of resonances are broadened or missing in the $^{1}H-^{15}N$ HSQC spectrum of Cu^{I}−CopK. These include V7, K8, Y10, K55, G56, E58, I59, F60, R61, L62, D63 and correspond to residues that occur in the dimer interface of the crystal structures of *apo*-CopK and Cu^{I}−CopK (Figures 11b, 12a). Their broadening is indicative of chemical exchange on an intermediate time scale under the conditions of the NMR experiment. The Cu^{I} binding appears to reduce order in the regions forming the dimer interface and to induce dimer dissociation in solution but not to abolish the dimer-monomer equilibrium completely. The dimeric form of Cu^{I}−CopK observed in the crystal structure suggests that the high protein concentration in the crystal (estimated at 75 − 100 mM) has driven the equilibrium back to the dimeric form (Figure 11a).

Titration of Cu^{I}−CopK with additional $[Cu^{I}(CD_3CN)_4]^{+}$ induced further changes in chemical shifts and additional resonance line broadening (Figure S9, Supporting Information), indicating that the interaction between Cu^{I}−CopK and the second equivalent of Cu^{I} is relatively weak. Addition of a total of three equivalents of Cu^{I} was required to saturate the Cu^{I} binding capacity of CopK at a concentration of 1.3 mM. These findings are consistent with a low affinity interaction and chemical exchange with a dissociation constant for the second Cu^{I} of the order of 10^{-3} M, too large to be biologically relevant. The suggestion of a stable Cu^{I}_2-CopK form is not tenable.[21]

Introduction of air into the CopK sample containing two equivalents of Cu^{I} led to rapid evolution of a set of new resonances (Figure 12b, red contours) that was identical to that for $Cu^{I}Cu^{II}$−CopK isolated by cation exchange chromatography (Figure 5c). It is apparent that $Cu^{I}Cu^{II}$−CopK was generated by oxidative trapping of the second equivalent of Cu^{I} (cf, Figure 2b). These results confirm that three separate forms of CopK exist (*apo*-CopK, Cu^{I}−CopK and $Cu^{I}Cu^{II}$−CopK) and they do not exchange on the NMR time scale.

The overall effects of metal binding on CopK were evaluated quantitatively by the weighted average of $^{1}H^{N}$-^{15}N chemical shifts ($\Delta_{av}(HN) = [(\Delta\delta_H^2 + \Delta\delta_N^2/25)/2]^{1/2}$),[35] shown in Figures 12c, d and Figure S10a (Supporting Information). Binding of the first equivalent of Cu^{I} perturbed the chemical shifts of amide resonances throughout CopK, and not just for those resonances derived from residues in close proximity to the metal ion (Figures 12a, c; $\Delta_{av}(HN) > 0.1$ ppm). This suggested that binding of Cu^{I} has induced a major structural change involving dimer dissociation in solution and consequently it was not possible to identify the Cu^{I} ligands unambiguously using NMR. Consistent with this conclusion, previous chemical shift analysis also indicated a less ordered secondary structure for Cu^{I}−CopK in solution and the presence of only five rather than seven β-strands as seen in the *apo* form.[21] In contrast, for the Met-rich copper binding proteins CopC from *P. syringae*, CusF from *E. coli* and DR1885 *from D. radiodurans*, addition of one equivalent of Cu^{+} induced a distinct pattern of chemical shift perturbation for those residues that were either directly involved in Cu^{I} binding or were in close proximity to the Cu^{I} ion, but caused minimal changes only for the remaining residues.[24,27,36] For these proteins, Cu^{I} binding perturbed the conformation of local Cu^{I} binding site, but not the overall structures. Consequently, the observation of essentially identical structures for *apo*-CopK and Cu^{I}−CopK in the solid state suggests that intermolecular hydrogen bonding interactions in the dimeric forms (at the high relative concentration in the crystals) have dominated the effect of Cu^{I} binding, effectively imposing the *apo* dimeric structure upon Cu^{I}−CopK in the solid state. Similar effects were observed for equivalent Ag^{I} binding in place of Cu^{I} (Figure S10b, c, Supporting Information).

Addition of one equivalent of Cu^{2+} to Cu^{I}−CopK induced further chemical shifts ($\Delta_{av}(HN) > 0.1$ ppm) for many residues throughout the molecule, with several becoming undetectable (Figures 12b, d and S10a, Supporting Information). This indicates high affinity binding of Cu^{II} to Cu^{I}−CopK. In contrast, titration of Cu^{2+} to *apo*-CopK decreased the resonance intensities of selected residues including His19 and His70 but caused little change in overall positions of the resonances, consistent with no major structural changes.[21] Both His residues are remote from each other in the NMR structure of *apo*-CopK and may be involved in separate weak and adventitious Cu^{II} binding.

(35) Garrett, D. S.; Seok, Y. J.; Peterkofsky, A.; Clore, G. M.; Gronenborn, A. M. *Biochemistry* **1997**, *36*, 4393–4398.
(36) Loftin, I. R.; Franke, S.; Roberts, S. A.; Weichsel, A.; Heroux, A.; Montfort, W. R.; Rensing, C.; McEvoy, M. M. *Biochemistry* **2005**, *44*, 10533–10540.

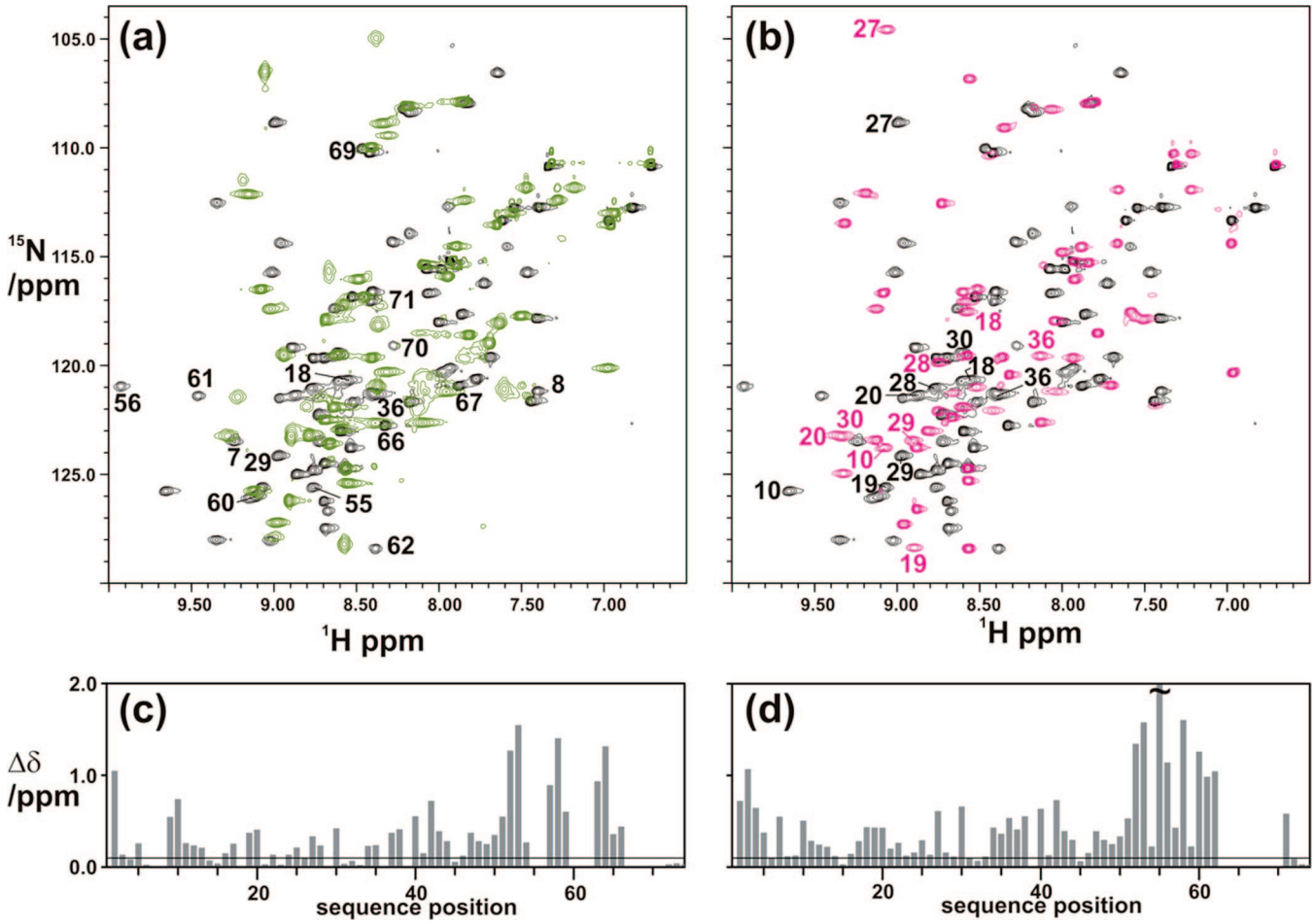

Figure 12. (a, b) Overlaid ^{1}H−^{15}N HSQC spectra of *apo*-CopK (black), Cu^{I}−CopK (green) and Cu^{I}Cu^{II}−CopK (pink) in KPi buffer (50 mM; pH 6.7; 5% D_2O). The protein concentrations are in the range of 1.0−1.5 mM. The resonances labeled in (a) are those in *apo*-CopK that are absent in the spectrum of Cu^{I}−CopK. Resonances labeled in (b) are those that have an amide nitrogen within 5 Å of H19 or E29. The numbers are color-coded as the spectra. The presence of these residues in (b) implies that H19 and E29 do not form the Cu^{II} binding site. (c, d) Weighted average chemical shift differences of amide resonances (Δ_{av}(HN) = $[(\Delta\delta_H^2 + \Delta\delta_N^2/25)/2]^{1/2}$) (line is at 0.1 ppm,): (c) between Cu^{I}−CopK and *apo*-CopK; (d) between Cu^{I}Cu^{II}−CopK and *apo*-CopK. Where there is no bar, an assignment of either protein is missing, except for residue P39 which lacks an amide proton.

However, high affinity Cu^{I} binding induced dimer dissociation with major structural changes in solution and this leads to the creation of a high affinity binding site specific for Cu^{II}.

Nature of the Cu^{II} Binding Site in Cu^{I}Cu^{II}−CopK. There is no sequence conservation characteristic of a Cu^{II} binding site in CopK or its sequence homologues (Figure 1). Absorbance and EPR spectra of the isolated Cu^{I}Cu^{II}−CopK samples indicate the presence of a type II Cu^{II} center with superhyperfine coupling to at least one ^{14}N ligand, most likely derived from either His19 or His70 (Figure 3).

In principle, it is possible to identify a Cu^{II}−His fragment from the electron relaxation effects of the paramagnetic Cu^{II} center on the resonances of the His side chain and of other adjacent nuclei (in reference to the resonances of the same sample in the absence of Cu^{II}).[37] Arnesano et al. estimated that ^{1}H, ^{13}C or ^{15}N resonances located within 11, 7 or 5 Å, respectively, of the Cu^{II} site will be severely broadened or missing due to rapid nuclear relaxation.[38] Resonances from His19 and the surrounding residues were clearly detected in the HSQC spectrum of Cu^{I}Cu^{II}−CopK while resonances from many residues in the C-terminal region including His70 were not (Figure 12). These observations suggest that the Cu^{II} ion is bound in the C-terminal region around His70, but not around His19. However, identification of the Cu^{II} binding site was hindered by the absence in the HSQC spectrum of Cu^{I}−CopK of resonances from many residues in the C-terminus, including His70. As discussed above (Figures 11b, 12a), this appears to be a consequence of the solution dimerization equilibrium in Cu^{I}−CopK inducing chemical exchange on an intermediate time scale. For clarification, the two protein variants H19F and H70F were generated. A preliminary copper binding study involving addition of Cu^{2+} to the Cu^{I} forms of these proteins confirmed that Cu^{I}−H19F, but not Cu^{I}−H70F, can bind Cu^{II}.[39] The result strongly suggests that His70 (in the C-terminal region), and not His19 (in the N-terminal region, is involved in the high affinity binding of Cu^{II} in Cu^{I}Cu^{II}−CopK in solution. The site would

(37) Bertini, I.; Luchinat, C.; Parigi, G.; Pierattelli, R. *ChemBioChem* **2005**, *6*, 1536–1549.
(38) Arnesano, F.; Banci, L.; Bertini, I.; Felli, I. C.; Luchinat, C.; Thompsett, A. R. *J. Am. Chem. Soc.* **2003**, *125*, 7200–7208.
(39) Two protein variants H19F and H70F were generated while this paper was under review. Experiments equivalent to those in Figure 5c led to the clean elution of the protein products as a single peak at positions expected for Cu^{I}Cu^{II}-H19F and Cu^{I}-H70F, respectively. The identities of both products were confirmed further by analysis of Cu^{I} and Cu^{II} content and by the finger-prints of their respective solution spectra (cf: Figures 3a and S3c, Supporting Information). A full characterization of all ligands involved in high affinity Cu^{I} and Cu^{II} binding in solution is in progress.

be assembled upon dissociation of dimeric forms of CopK but it should be noted that the binding cooperativity between Cu^{I} and Cu^{II} is not dependent upon the monomer−dimer equilibrium in solution (see Figures 2b and S6a, Supporting Information).

Summary and Structural Implications for Binding Cooperativity. Experiments in solution confirmed that *apo*-CopK binds Cu^{I} with high affinity (K_D, 2×10^{-11} M) but Cu^{II} with low affinity ($K_D > 10^{-6}$ M) and that these affinities are independent of the solution state (monomer versus dimer). However, binding of Cu^{I} increases $K_D(Cu^{II})$ by a factor of at least 10^6 whereas binding of Cu^{II} increases $K_D(Cu^{I})$ by a factor of $\sim 10^2$. This binding cooperativity ensures that monomeric $Cu^{I}Cu^{II}$−CopK is a stable molecule in air.

Apo-CopK exists as a dimer in solution ($K_D \approx 10^{-5}$ M). NMR[21] and crystal structures confirm the dimeric state in both solution and solid state and reveal a β-sandwich structure composing of two antiparalled β-sheets. The crystal structure confirms further that 14 intermolecular hydrogen bonds contribute to dimer formation with the C-terminal β-strands contributing strongly to the dimer interface. Both His19 and His70 may participate in separate weak Cu^{II} binding but such interactions do not alter the overall structure nor cause dimer dissociation. However, high affinity Cu^{I} binding shifts the monomer−dimer equilibrium and releases residues in the dimer interface with considerable structural perturbation in solution. This leads to the creation of a high affinity binding site specific for Cu^{II}.

The presence of significant intermolecular interaction increased molecular dynamics and restricted the structural information available from NMR spectroscopy. The high protein concentration in the crystals apparently favors the dimeric *apo*-CopK form over monomeric forms. This factor appears to contribute to the loss of Cu^{II} upon crystallization of $Cu^{I}Cu^{II}$−CopK and crystallization of a dimeric Cu^{I}−CopK with a structure which essentially superimposes upon that of the *apo*-CopK dimer. Binding of Cu^{I} by the cluster of conserved methionine residues in a small hydrophobic core ensured that it remained the highest affinity Cu^{I} site in the crystals. Intermolecular interactions appear to be abolished for $Cu^{I}Cu^{II}$−CopK in solution with the Cu^{II} ion evidently bound in the C-terminal region. The observed binding cooperativity between Cu^{I} and Cu^{II} may be associated with the flexibility of the β-sandwich structure which also leads to the well-developed intermolecular interactions observed in both the solution and the solid states.

Implications for Biological Function. The high copper resistance of bacterium *C. metallidurans* CH34 is attributed largely to the presence of a *cop* cluster of 19 genes on the plasmid pMOL30 that respond to environmental copper stress. Products of the *cop* cluster include six Cop proteins (CopABCDRS) which are close homologues of those encoded by *pco/cop* operons in copper resistant strains of *E. coli* and *P. syringae* pathovar *tomato* (see Introduction). These Pco/Cop proteins provide a basic resistance mechanism for removing excess copper from the periplasm of these copper resistant bacteria. CopK is a soluble periplasmic protein encoded by the *cop* cluster of pMOL30 but has no homologue in the Pco/Cop systems. Expression of both CopK and CopC in *C. metallidurans* CH34 is strongly up-regulated by copper salts and both proteins accumulate to high concentrations in the periplasm under copper stress.[20] They each bind Cu^{I} and Cu^{II} at separate sites to form the air-stable complexes $Cu^{I}Cu^{II}$−CopK and $Cu^{I}Cu^{II}$−CopC. However, as documented in this work, the copper chemistries

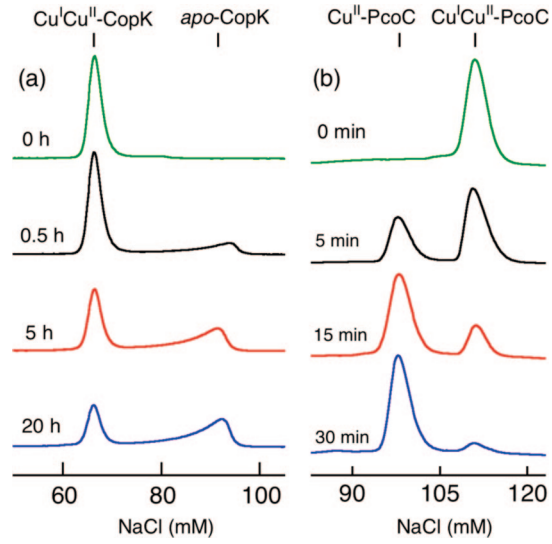

Figure 13. Oxidation of protein-bound Cu^{I} by air catalyzed by *holo*-PcoA in air-saturated Mops buffer (20 mM; pH 7; $NaNO_3$, 100 mM): (a) $Cu^{I}Cu^{II}$−CopK (50 μM) and *holo*-PcoA (2 μM); (b) $Cu^{I}Cu^{II}$−PcoC (25 μM) and *holo*-PcoA (0.5 μM). The progress of the reactions was analyzed on a Mono-S HR 5/5 cation exchange column at reaction intervals as indicated. The catalytic oxidation rate in (a) was at least 20 times slower than that in (b).[13] In fact, *holo*-PcoA was not able to complete the catalytic oxidation of Cu^{I} in $Cu^{I}Cu^{II}$−CopK (molar ratio 1: 25) at the catalytic lifetime of *holo*-PcoA ($t_{1/2} \approx 20$ h) under the reaction conditions. Oxidation of $Cu^{I}Cu^{II}$−CopK led to a loss of both Cu^{I} and Cu^{II}, but oxidation of $Cu^{I}Cu^{II}$−PcoC led to a loss of Cu^{I} only.

of the two proteins are distinctly different. Reactions of $Cu^{I}Cu^{II}$−CopK and $Cu^{I}Cu^{II}$−PcoC with the cuprous oxidase PcoA in air-saturated buffers were compared to test whether CopK might substitute functionally for CopC/PcoC as a substrate for CopA/PcoA. The experiments in Figure 13 demonstrated clearly that air-oxidation of Cu^{I} in $Cu^{I}Cu^{II}$−CopK catalyzed by PcoA was at least 20 times slower than the equivalent reaction with $Cu^{I}Cu^{II}$−PcoC,[13] although the $K_D(Cu^{I})$ values in both $Cu^{I}Cu^{II}$−CopK and $Cu^{I}Cu^{II}$−PcoC are similar (Figure 8). $^{1}H-^{15}N$ HSQC spectroscopy was employed to monitor interactions of ^{15}N-labeled $Ag^{I}Cu^{II}$−CopK and ^{15}N-labeled $Ag^{I}Cu^{II}$−PcoC (unreactive analogs of the $Cu^{I}Cu^{II}$ proteins) with unlabeled *holo*-PcoA. The HSQC spectrum of $Ag^{I}Cu^{II}$−CopK was unaffected by the presence of 2 equivalents of PcoA (see Figure S11, Supporting Information) whereas that of $Ag^{I}Cu^{II}$−PcoC experienced significant line broadening such that the resonances became undetectable.[40] This suggests that the cuprous oxidase PcoA interacts directly and specifically with $Ag^{I}Cu^{II}$−PcoC, but not with $Ag^{I}Cu^{II}$−CopK.

These experiments suggest that CopK and CopC, the two most inducible soluble periplasmic proteins, play different roles in copper resistance. Uncharacterized members of the *cop* cluster in pMOL30 include a transmembrane P1-type ATPase CopF and several cysteine-containing cytosolic proteins (CopJ, CopG, CopL) that may work collectively to supplement the function of the chromosomal Cu^{I} translocating P-type ATPase CopA in removing Cu^{I} from the cytoplasm. This, in turn, may require additional periplasmic proteins such as CopK and CopH[41] to cope with the increased copper stress in the periplasm. They may simply scavenge Cu^{I} and/or Cu^{II} from the periplasm and

(40) Djoko, K. Y.; Hinds, M. G.; Xiao, Z.; Wedd, A. G. Unpublished results.
(41) Sendra, V.; Cannella, D.; Bersch, B.; Fieschi, F.; Menage, S.; Lascoux, D.; Coves, J. *Biochemistry* **2006**, *45*, 5557–5566.

transfer them directly to outer membrane bound proteins such as CopB. Notably, the outer membrane bound protein CopB (encoded by the *cop* cluster in pMOL30) features a unique N-terminus.[20] It comprises ten identical methionine-rich motifs (**MQGMDHSKMQGM**DQGS) that may function as a Cu^{I}/Cu^{II} sponge to extract Cu^{I}/Cu^{II} from CopK and other periplasmic copper binding proteins. Together, they may supplement the function of CusABCF in copper resistance, especially under anaerobic conditions.

Experimental Section

Expression Plasmid. A DNA sequence encoding full-length CopK protein from *C. metallidurans* CH34,[20] including leader sequence, was synthesized by assembly of PCR products[42] with codons optimized for protein expression in *E. coli*. Restriction sites *Nde*I and *Bam*HI were introduced up- and downstream, respectively, of the synthetic gene to facilitate cloning into the expression vector pET20b (Novagen). An insertion of the correct CopK gene into the expression vector created the expression plasmid *p*CX07 that was confirmed by DNA sequencing analysis and protein expression.

Protein Expression and Purification. Plasmid *p*CX07 was propagated with *E. coli* DH5α and transformed into *E. coli* BL21(DE3) for expression of wild type CopK. Each 1 L of 2YT medium containing ampicillin (100 mg) was inoculated with an overnight culture (10 mL) of BL21(DE3) cells containing the expression plasmid. After the cells were grown aerobically with vigorous shaking at 37 °C to OD_{600} ~1, isopropyl-β-D-thiogalactopyranoside (IPTG) was added to a final concentration of 0.4 mM to induce protein expression. Following further cell growth and protein induction at ~30 °C for 2−4 h or at room temperature (~22 °C) overnight, cells were harvested by centrifugation. A clarified lysis extract was prepared in Tris-HCl buffer (where Tris = tris(hydroxymethyl)aminoethane) (20 mM; pH 8) containing Edta (1 mM). Negatively charged *E. coli* proteins were removed by passing the clarified lysate through a DE-52 anion exchange column in Tris-HCl buffer (20 mM; pH 8). The flow-through fraction that contained CopK protein was adjusted to pH 6 with 2-(*N*-morpholino)ethanesulfonic acid (Mes) (0.2 M) and applied to a CM-52 cation exchange column in a Mes buffer (20 mM; pH 6). The bound proteins were eluted with a salt gradient of 0−0.3 M NaCl in the same Mes buffer. Edta (1 mM) was included in the buffer to ensure removal of contaminating metal ions. *Apo*-CopK was eluted as a single peak at 0.19−0.25 mM NaCl. The final purification step used a Superdex-75 gel filtration column (HR10/30; Amersham Bioscience) with an eluent buffer (20 mM; 100 mM NaCl) of KPi (pH 6.7) or Mops (pH 7) to remove Edta and minor components of other contaminant proteins. The purity and identity of the isolated CopK protein were confirmed by SDS-PAGE (Figure S1, Supporting Information) and ESI-MS (Figure S2, Supporting Information). The isolated protein was in its *apo* form with no detectable copper content (yield ~ 50 mg per L of culture).

An isotope-enriched sample was produced similarly from cells grown in a M9 minimal medium supplemented with ^{15}N-NH_4Cl and ^{13}C-glucose. ESI-MS data confirmed an average of 94% incorporation of both labels.

Generation and Analysis of Metalated Forms. Aqueous $CuSO_4$ in the presence or absence of NH_2OH (~1 mM) or $[Cu^{I}(CH_3CN)_4]ClO_4$ in CH_3CN was added quantitatively to solutions of *apo*-CopK. Incubation was followed by gel filtration on an Econo-Pac 10DG desalting column (Bio-Rad) to remove unbound copper ions. The copper content of protein samples was determined spectrophotometrically by reaction with the Cu^{I}-specific colorimetric reagent Bcs as described previously.[17] The Cu^{I} content was determined initially and the total copper content (and hence the Cu^{II} content by difference) after subsequent addition of reductant dithionite to the same solution. The data were confirmed by independent analysis via inductively coupled plasma mass spectrometry (ICP-MS). Various metalated forms were also generated and analyzed by cation exchange chromatography and the identities confirmed by copper analysis and by ESI-MS under nondenaturing conditions (see Figure 5 and Table 2). Metalation with other metal ions such as Ag^{+}, Ni^{2+}, Co^{2+}, Zn^{2+}, Cd^{2+}, and Hg^{2+} was effected similarly and the products examined by cation exchange chromatography.

Concentration Assays. Stock solutions of Cu^{+}, Cu^{2+} and Bca were standardized according to protocols described previously.[15] The concentration of *apo*-CopK was estimated from solution absorbance using ϵ_{280} = 1,500 M^{-1} cm^{-1} as determined by quantitative drying of protein samples in the volatile buffer NH_4HCO_3. This value is consistent with that calculated from the protein amino acid content (ϵ_{280}, 1,490 M^{-1} cm^{-1}). A value of ϵ_{280} = 3,100 M^{-1} cm^{-1} for $Cu^{I}Cu^{II}$−CopK was estimated by titration of 2 equivalent of Cu^{2+} into *apo*-CopK (100 μM) solution in Mops buffer (50 mM; pH 7) in the presence of NH_2OH (1 mM). This value was confirmed by copper analysis of the isolated samples (see Table 2).

ESI-MS Analysis. Spectra were recorded on an Agilent Q-TOF mass spectrometer (Model 6510) in positive ion mode with capillary voltage set at 4000 V, fragmentor voltage at 150 V and skimmer voltage at 70 V. The drying gas was held at 100 °C. Protein samples (~10 μM) were prepared in 50% MeOH containing 0.1% formic acid for analysis under denaturing conditions and in 50 mM ammonium formate (pH ~ 7) for analysis under nondenaturing conditions. For the latter analysis, the samples were delivered continuously to the electrospray probe at a flow rate of 10−20 μL min^{-1} via a syringe pump. Spectra were recorded at a scan rate of 2 s/scan from 100−3200 *m*/*z* for 2−3 min and then averaged. The average molar masses were obtained by applying a deconvolution algorithm to the recorded spectra and were calibrated internally with Agilent API-TOF reference mass solution kit.

Other Biophysical Analysis. UV−visible spectra were recorded on a Varian Cary 300 spectrophotometer in dual beam mode with quartz cuvettes of 0.5 or 1 cm path length. Steady-state fluorescence spectra were obtained on a Varian Cary Eclipse spectrophotometer. For fluorescence emission spectra, the excitation wavelength was 280 nm with a bandpass of 10 nm for both excitation and emission spectra. The spectra were recorded between 295 − 500 nm at a scan rate 600 nm/min. The absorbance of protein solutions was maintained below A_{280} = 0.1 to minimize resorption effects.

Sedimentation equilibrium experiments were carried out at 20 °C using a Beckman Optima XL-A analytical ultracentrifuge with an An-Ti60 rotor. All samples (0.2 mM) were prepared in Mops buffer (10 mM, pH 7). Ag^{I}−CopK and $Cu^{I}Cu^{II}$−CopK were prepared by elution from the Mono-S column (Figure 5c). To minimize interference from potential redox chemistry, both Cu^{I}−CopK and "Cu^{II}−CopK" were prepared just before the sedimentation experiments. Cu^{I}−CopK was prepared in the anaerobic glovebox by titration of 1.0 equivalent of $[Cu^{I}(CH_3CN)_4]^{+}$ into *apo*-CopK and "Cu^{II}−CopK" by titration of 2.0 equiv of Cu^{2+} into *apo*-CopK. Sedimentation equilibrium distributions were determined from radial scans at 280 nm. The final equilibrium distributions were fitted globally using the program SEDEQ1B (kindly provided by Allen Minton, NIH, Bethesda, MD). The partial specific volume of the protein (0.72 mL/g) was calculated from the amino acid composition.

Estimation of Cu^{I} Binding Affinities. Two independent approaches were employed. The first involved competition for Cu^{I} between the protein and chromophoric ligand Bca according to eq 4. In the presence of excess ligand, the absorbance of $[Cu^{I}(Bca)_2]^{3-}$ in the UV−visible region (λ_{max} 562 nm, ϵ 7,900 M^{-1} cm^{-1}; λ_{max} 358 nm, ϵ 42,900 M^{-1} cm^{-1}; see Figure 7)[15] allowed quantification of its equilibrium concentration which depends upon both [Bca] and [CopK] in reaction 4. The dissociation constant $K_D(Cu^{I})$ for Cu^{I}−CopK was estimated via eq 5 with a reported $\beta_2 = 10^{17.2}$ M^{-2} for $[Cu^{I}(Bca)_2]^{3-}$.[28] The other terms in eq 5 are the equilibrium

(42) Stemmer, W. P.; Crameri, A.; Ha, K. D.; Brennan, T. M.; Heyneker, H. L. *Gene* **1995**, *164*, 49–53.

concentrations that were calculated from the respective total concentrations and the observed $[Cu^{I}(Bca)_2]^{3-}$ concentration.

Experiments were conducted under anaerobic conditions in Tris-Mes buffer (20 mM; pH 8; NaCl, 100 mM) according to a previous protocol with some modifications.[15,30] Briefly, reaction 4 was explored by adding varying quantities of *apo*-CopK protein under anaerobic conditions to a solution containing $[Cu^{I}(Bca)_2]^{3-}$. This was prepared by mixing $[Cu^{I}(CH_3CN)_4]ClO_4$ and Bca in a molar ratio of 1:3 to ensure that all Cu^{I} not bound to protein was present as $[Cu^{I}(Bca)_2]^{3-}$. Asc was included in each reaction to ensure elimination of trace Cu^{2+}. Aliquots of each reaction mixture were diluted to 1 mL for recording of the solution spectrum which remained unchanged for at least 10 min. The dilutions were controlled so that the same total concentrations of Cu^{I}, Bca and Asc were present in all solutions after the dilutions. To ensure correct readings of the absorbance at 358 nm, it was important to use a solution reference that contained equimolar Bca in the same buffer.[15] Reaction stoichiometries and $K_D(Cu^{I})$ for *apo*-CopK derived via eq 5 are given in Table 3, expt 1.

However, the affinity of CopK for Cu^{I} increased in the presence of Cu^{2+}, as shown by the observed drop on both A_{358} and A_{562} upon introduction of Cu^{2+} into the competing system. Addition of the same amount of Cu^{2+} into the control solution lacking CopK had negligible impact for at least 5 h under anaerobic conditions (Figure 7). The presence of excess Cu^{2+} in the system ensured that any high affinity Cu^{II} sites on the protein were saturated rapidly, preventing oxidative trapping by the protein of Cu^{I} in $[Cu^{I}(Bca)_2]^{3-}$. In addition, possible slow reduction of Cu^{2+} by *apo*-CopK (see Figure S7, Supporting Information) was not observed on the experimental time scale ($\sim$ 2 h) under the conditions. This may be attributed to the weak but significant Cu^{II} binding affinity of the Tris-Mes buffer and/or of the ligand Bca. These two experimental facts minimized redox interference between Cu^{I} and Cu^{II} and allowed the competition of reaction 6 to be quantified according to eq 7. Strong binding cooperativity between Cu^{I} and Cu^{II} ensured that $Cu^{I}Cu^{II}$−CopK was the dominant Cu^{I}-containing protein species with a negligible contribution from Cu^{I}−CopK under the conditions of excess Cu^{2+}, (ie, $[Cu^{I}Cu^{II}-CopK] = [Cu^{I}]_{total} - [Cu^{I}(Bca)_2{}^{3-}]$). *Apo*-CopK binds Cu^{2+} weakly ($K_D(Cu^{II}) > 10^{-6}$ M) and an intact Cu^{II}−CopK form could not be isolated. However, by defining "Cu^{II}−CopK" as the total CopK species that do not bind Cu^{I}, (ie, ["Cu^{II}−CopK"] = $[CopK]_{total} - [Cu^{I}Cu^{II}-CopK]$), it was possible to quantify an apparent $K_{D6}(Cu^{I})$ for CopK that is dependent on the availability of Cu^{2+} (see eqs 6, 7). In fact, competition in the presence of Asc as defined by eqs 4, 5 is just a special case of the competition defined by eqs 6, 7 where the Cu^{2+} availability is eliminated.

Experiments in the presence of Cu^{2+} were also carried out under strict anaerobic conditions. Asc was excluded from the system and Cu^{2+} was introduced by premixing with *apo*-CopK in 1:1 ratio (Table 3, expt 2) in Tris/Mes buffer (20 mM; pH 8; NaCl, 100 mM). The data in Table 3 clearly indicated an increase in the affinity of CopK for Cu^{I} when Cu^{2+} was available for co-binding.

Equivalent experiments on the PcoC protein from *E. coli* failed to detect similar effects. PcoC features two separate binding sites specific for Cu^{I} and Cu^{II} and binds either Cu^{I} or Cu^{II}, or both, with high affinity ($K_D \approx 10^{-13}$ M for both sites).[15]

The second approach was based on competition for Cu^{I} between CopK and Cu^{II}−PcoC. The latter binds Cu^{I} ($K_D \approx 10^{-13}$ M) but has little affinity for Cu^{II} (since the Cu^{II} site is occupied).[15] Again, the competition was conducted in the presence and absence of Cu^{2+} under anaerobic conditions and reaction mixtures were separated and identified by elution on the Mono-S cation-exchange column. The results are displayed in Figure 8.

Estimation of Ag^{I} Binding Affinities. CopK proteins with Ag^{I} bound in place of Cu^{I} were isolated as Ag^{I}−CopK and $Ag^{I}Cu^{II}$−CopK. The binding affinities of Ag^{I} in both forms were compared, respectively, with those of Cu^{I} analogues by competition for Cu^{+}. The experiments were carried out under anaerobic conditions by following the changes in solution spectra upon titration of Cu^{+} into solutions of Ag^{I}−CopK and $Ag^{I}Cu^{II}$−CopK. In separate experiments, equimolar silver acetate and $[Cu^{I}(CH_3CN)_4]ClO_4$ (each 1.1 eq) were added, in two different orders, to two separate solutions of *apo*-CopK, followed by Cu^{2+} (1.5 equiv) in each case. After removal of unbound metal ions by recovering the total protein components as a single elution peak on a Mono-S column (Figure 5c), the compositions of protein components were estimated by analysis of copper contents.

Estimation of Cu^{II} Binding Affinities. The affinities of CopK for Cu^{II} depend on the availability of Cu^{+} or Ag^{+} for co-binding. In the absence of either ions, the affinity was weak and could be estimated directly from titration of *apo*-CopK with Cu^{2+} in buffers that bind Cu^{2+} weakly (Mops, Tricine; see Figures 2 and S3). However, in the presence of these ions, the affinity increased dramatically and a quantitative estimation required competition with a stronger Cu^{II} ligand of known affinity. A CopC triple variant with a disabled Cu^{I} site (■□-CopC) was chosen for the competition according to eq 11 and $K_D(Cu^{II})$ for Cu^{I}−CopK calculated according to eq 12. The dissociation constant $K_D(Cu^{II}) = 7.2 \times 10^{-14}$ M for ■□-CopC was determined previously in ref[17] which also provides details of the derivation of eq 11. When reaction 11 is appropriately competitive, the equilibrium concentration $[Cu^{I}Cu^{II}-CopK]$ equals the loss of Cu^{II} from ■Cu^{II}−CopC. This was determined experimentally as described below and provides the other terms in eq 12 as well.

The *apo* forms of CopK and CopC both fluoresce when excited at 280 nm. There is a slight difference in the emission maxima but a considerable difference in the intensities under the same conditions (F_{324}(CopC)/F_{309}(CopK) = 7.6:1; see Figure 9a). More importantly, Cu^{II} binding quenched the fluorescence intensities of both proteins but ΔF at 320 nm induced by reaction 11 is dominated by the contribution from the CopC protein (ΔF_{CopC}:ΔF_{CopK} = 20:1; see Figure 9a). Therefore, the ΔF_{obs} at 320 nm due to Cu^{II} transfer in eq 11 can be taken as a good measure of ΔF_{CopC} only (ie, $\Delta F_{obs} = \Delta F_{CopC} + \Delta F_{CopK} \approx \Delta F_{CopC}$). However, Cu^{I}−CopK is air-sensitive, particularly under the Cu^{II} competition conditions, and has to be generated *in situ* from *apo*-CopK for a reliable estimation of ΔF_{CopC}. Consequently, a precompetition solution containing Cu^{2+}, ■□-CopC and *apo*-CopK was prepared initially and the emission spectra recorded. A control with $[Cu^{II}]/[■□\text{-CopC}] < 1$ ensured that all Cu^{2+} ions were bound as ■Cu^{II}−CopC because *apo*-CopK could not compete for Cu^{II} under the conditions. Reaction 11 was initiated by addition of a substoichiometric amount of Cu^{+} (relative to *apo*-CopK) into the initial solution and the emission spectra recorded again after establishment of equilibrium (<5 min). The disabled Cu^{I} site in ■□-CopC was confirmed to be unable to compete for Cu^{I} with *apo*-CopK under the conditions. Thus the concentration of added Cu^{+} was equal to the total concentration of Cu^{I}−CopK and $Cu^{I}Cu^{II}$−CopK. An increase in F_{320} after the addition of Cu^{+} demonstrated an effective competition for Cu^{II} between Cu^{I}−CopK and ■□-CopC.

However, the approach was complicated by the increase in ΔF_{320} of CopK upon conversion of dimeric *apo*-CopK to monomeric Cu^{I}−CopK (i.e., $\Delta F_{obs} = \Delta F_{CopC} + \Delta F_{D\text{-}M}$; see Figures 2b, S6, Supporting Information). The latter contribution $\Delta F_{D\text{-}M}$ became more significant as the affinity of Cu^{I}−CopK for Cu^{II} was found to be weaker than that of ■□-CopC and so excess Cu^{I}−CopK was required to effect the competition (eq 11). It was noted that the binding of Ag^{I} to CopK had the same effect on $\Delta F_{D\text{-}M}$ (see Figure S6, Supporting Information) but that the affinity of Ag^{I}−CopK for Cu^{II} not high enough to compete for Cu^{II} with ■□-CopC. Thus, addition of Ag^{+} into the precompetition solution caused *apo*-CopK dimer dissociation, but no competition for

(43) This was confirmed by two experimental observations: (i) at lower CopK concentration at which *apo*-CopK dimer was largely dissociated, addition of Ag^{+} into the precompetition solution caused almost no change in F_{320} (see Table 4, expt 4); (ii) the protein species detected by native ESI−MS from the solution after Ag^{+} addition included Ag^{I}−CopK, *apo*-CopK and Cu^{II}-CopC, but no $Ag^{I}Cu^{II}$−CopK.

Cu^{II} (i.e., $\Delta F_{obs} = \Delta F_{D\text{-}M}$ in this case),[43] consistent with a shift of the peak maximum toward that of CopK direction after addition of Ag^+ (see Figure 9b(ii)). An equivalent experiment with Cu^+ more than doubled ΔF_{obs} but with little shift in the peak maximum, consistent with that $\Delta F_{obs} = \Delta F_{CopC} + \Delta F_{D\text{-}M}$ (Figure 9b(iii)). Therefore, ΔF_{CopC} was obtained from ΔF_{obs} with background subtraction from the equivalent experiment with Ag^+. Addition of 10 equiv of Edta into the same precompetition solution ensured complete removal of all bound Cu^{II} from ■Cu^{II}−CopC but with little effect on *apo*-CopK, as was also indicated by the shift of the peak maximum in the CopC direction (Figure 9b(iv)). A comparison of ΔF_{CopC} vs ΔF_{Edta} allowed a quantitative estimation of the fraction of Cu^{II} transferred from ■Cu^{II}−CopC to Cu^{I}−CopK and thus of $K_D(Cu^{II})$ for Cu^{I}−CopK from eq 12. Details of the experiments and the results are given in Table 4.

It is emphasized, however, that the observed increase in F_{320} must be treated as a minimum value, because the competition solution was highly air-sensitive and the Cu^I in Cu^{I}−CopK may be oxidatively trapped by the high-affinity Cu^{II} site in ■□-CopC as stable ■Cu^{II}−CopC and this will offset the increase in F_{320}. Therefore, strict anaerobic conditions and rapid equilibration (<5 min) were the keys to the observation of the competition of eq 11. Indeed, this is the first example of determination of $K_D(Cu^{II})$ for an air-sensitive Cu^I species (Cu^{I}−CopK).

Interaction between $Cu^{I}Cu^{II}$−CopK and the Cuprous Oxidase PcoA. PcoA from *E. coli* catalyzes air oxidation of Cu^I bound in $Cu^{I}Cu^{II}$−PcoC via direct molecular interaction.[13] To investigate a possible role of CopK in copper resistance, similar experiments were carried out between $Cu^{I}Cu^{II}$−CopK and PcoA. The reaction was started by incubation at 25 °C of a mixture consisting of *holo*-PcoA (2 μM) and $Cu^{I}Cu^{II}$−CopK (50 μM) in three air-saturated buffers at pH = 5, 6 and 7. Oxidation of $Cu^{I}Cu^{II}$−CopK was followed by separation of the protein products on the Mono-S cation exchange column.

X-Ray Crystallography. Crystal Growth and Analysis. Conditions for the crystallization of the *apo*-CopK and $Cu^{I}Cu^{II}$−CopK proteins (30 mg/mL, 21 mg/mL, respectively) were screened at 293 K according to the sparse-matrix method using commercially available screens and the hanging-drop vapor-diffusion technique.[44] Screens were set up in 96-well plates (F-bottom Microplates, Greiner) using a Mosquito nanoliter liquid handling robot (TTP LabTech). Equal volumes of protein (100 nL) and reservoir were mixed. For *apo*-CopK, small crystals were observed in condition 44 of the Classics screen (Qiagen, 0.1 M HEPES sodium salt pH 7.5, 1.4 M sodium citrate). Further refinement of the crystallization conditions produced crystals of typical dimensions 100 × 50 × 20 μm which were grown at room temperature by mixing protein solution (1 μL, 30 mg/mL) with an equal volume of reservoir solution (1.4 M sodium citrate, 0.1 M Na HEPES, pH 7.6). Crystallization experiments with $Cu^{I}Cu^{II}$−CopK produced crystals in condition 81 of the JCSG screen (Molecular Dimensions, 0.1 M KSCN, 30% (w/v) PEG MME 2000). Further refinement of the crystallization conditions produced crystals of typical dimensions 100 × 50 × 50 μm, which were grown at room temperature by mixing protein solution (1 μL, 21 mg/mL) with an equal volume of reservoir solution (0.1 M KSCN, 32% PEGMME 2000).

Crystals of *apo*-CopK were transferred directly into a cold N_2 gas stream (100 K) for data collection following brief (10 s) immersion in the appropriate cryoprotectant solution (1.4 M sodium citrate, 0.1 M Na HEPES, pH 7.6, 30% glycerol). Crystals of Cu-CopK were found to be adequately cryoprotected when frozen directly from the crystallization drop. X-ray diffraction data were recorded on a Mar345 image-plate detector with Cu Kα X-rays from a Rigaku RU-200 rotating anode generator focused using Osmic mirror optics. All data were processed and scaled with the *HKL* suite of programs, *DENZO* and *SCALEPACK*.[45] Statistics for the data collections are presented in Table 5.

Structure Solution and Refinement. The structure of Cu^{I}−CopK was solved by single wavelength anomalous dispersion phasing (SAD). The coordinates of the lowest energy model of *apo*-CopK, as determined by NMR (PDB entry 2k0q)[21] was used as a molecular replacement model in *PHASER*.[46] The position of a single molecule of CopK per asymmetric unit was solved with a translation function Z score of 5.8 and log-likelihood gain (LLG) of 24. The model phases from this solution allowed the positions of 8 sulfur atoms per asymmetric unit to be deduced from an anomalous difference Fourier map. In order to avoid model bias, the NMR model was used no further in the structure solution. The 8 sulfur atom positions were refined and SAD phases calculated using *SHARP*.[47] Solvent flattening was carried out with *DM*[48] to the resolution limit of the data, 1.55 Å. This produced a readily interpretable electron density map. Model tracing was carried out automatically with *ARP/wARP*,[49] which yielded a model consisting of residues 4−61. After initial rounds of refinement using *REFMAC5*,[50] the positions of a single Cu atom and two SCN^- ions were clearly visible in difference Fourier electron density maps (19, 13 and 4 σ peaks, respectively). Manual adjustments to the model and the addition of residues 1−3 and 62−66 were made using *COOT*.[51] Refinement was completed using *REFMAC5* with TLS.[50,52]

A single CopK molecule from the Cu^{I}−CopK structure, with the copper atom, SCN^- ions and water molecules removed, was used as the search model to find the position and orientation of one molecule of CopK within the asymmetric unit of the *apo*-CopK crystals. The molecular replacement was carried out with *PHASER*[46] and the refinement with *REFMAC5*.[50] For both structures, water molecules were added automatically using *ARP/wARP*[49] and confirmed by inspection of electron density maps in *COOT*[51] after consideration of conservative hydrogen-bonding criteria. All figures were generated using *PyMOL*.[53]

NMR Spectroscopy and Spectral Assignments. NMR experiments were carried out on samples (1.0−1.5 mM) enriched in ^{13}C and ^{15}N which were prepared in KPi buffer (50 mM; pH 6.7) containing ∼5% D_2O. Edta (3 mM) and NaN_3 (0.04%) were included in the *apo*-CopK sample to remove adventitious metal ions and inhibit bacterial attack. The $Cu^{I}Cu^{II}$−CopK sample was prepared by reaction of *apo*-CopK with Cu^{2+} (2.5 equiv) in the presence of NH_2OH, followed by separation on the Mono-S column. The Cu^{I}−CopK sample was obtained by quantitative anaerobic titration of Edta-free *apo*-CopK in an NMR tube with $[Cu^{I}(CD_3CN)_4]^+$ (1.0 equiv). The final CD_3CN content of 4% was demonstrated to have a negligible influence on the spectra. The solution of $[Cu^{I}(CD_3CN)_4]^+$ in CD_3CN was prepared by dissolving $[Cu^{I}(CH_3CN)_4]ClO_4$, followed by lyophilization and redissolving the solid residue in CD_3CN. Ag^{I}−CopK was prepared by titration of 1.1 equivalent of silver acetate into *apo*-CopK in Mops buffer, followed by separation on Mono-S column in KPi (10 mM; pH 6.7) with Na_2SO_4 as eluent.

Spectra were recorded at 25 °C on a Bruker DRX 600 spectrometer equipped with triple resonance probes and pulsed field gradients operating at 600 MHz, or AV-500 and AV-800 spectrometers equipped with a cryogenically cooled probes,

(44) Jancarik, J.; Kim, S. H. *J. Appl. Crystallogr.* **1991**, *24*, 409–411.
(45) Otwinowski, Z.; Minor, W. *Methods Enzymol.* **1997**, *276*, 307–326.
(46) McCoy, A. J.; Grosse-Kunstleve, R. W.; Adams, P. D.; Winn, M. D.; Storoni, L. C.; Read, R. J. *J. Appl. Crystallogr.* **2007**, *40*, 658–674.
(47) Vonrhein, C.; Blanc, E.; Roversi, P.; Bricogne, G. *Methods Mol. Biol.* **2007**, *364*, 215–230.
(48) Cowtan, K. *Jt. CCP4 ESF-EACBM Newslett. Protein Crystallogr.* **1994**, *31*, 34–38.
(49) Perrakis, A.; Morris, R.; Lamzin, V. S. *Nat. Struct. Biol.* **1999**, *6*, 458–463.
(50) Murshudov, G. N.; Vagin, A. A.; Dodson, E. J. *Acta Crystallogr. D: Biol. Crystallogr.* **1997**, *53*, 240–255.
(51) Emsley, P.; Cowtan, K. *Acta Crystallogr. D: Biol. Crystallogr.* **2004**, *60*, 2126–2132.
(52) Painter, J.; Merritt, E. A. *Acta Crystallogr. D: Biol. Crystallogr.* **2006**, *62*, 439–450.
(53) DeLano, W. L. *The PyMOL Molecular Graphics System*; DeLano Scientific: San Carlos, CA, 2002; http://www.pymol.org.

operating at 500 and 800 MHz respectively. A series of heteronuclear 3D NMR experiments were recorded using $^{13}C/^{15}N$ double labeled CopK proteins.[34] Spectra were processed using TOPSPIN (Bruker AG) and analyzed using XEASY.[54]

Acknowledgment. We thank the Australian Research Council for financial support under Grant A29930204. M.J.M. is a Cancer Institute of NSW Career Development Fellow. L.X.C. and M.-R.A. are recipients of Australian Postgraduate Awards. We thank Chak Ming Sze for assistance with ESI-MS experiments, Karrera Djoko for the experiments in Figure 13, Mr. Tim Ryan and Assoc. Prof. Geoffrey Howlett for sedimentation experiments, and Dr. Simon Drew for EPR measurements. NMR data were acquired at the Bio21 Institute NMR facility, Melbourne.

Supporting Information Available: Protein characterization data (structural analysis statistics; SDS-PAGE; ESI−MS; electronic spectra; sedimentation analysis; gel filtration chromatography; $^{1}H-^{15}N$ HSQC spectra: Tables S1−S2; Figures S1−S11). This material is available free of charge via the Internet at http://pubs.acs.org.

JA807354Z

(54) Bartels, C.; Xia, T. H.; Billeter, M.; Guntert, P.; Wuthrich, K. *J. Biomol. NMR* **1995**, *6*, 1–10.